Agricultural and Forest Meteorology 263 (2018) 346–361

Contents lists available at ScienceDirect

Agricultural and Forest Meteorology

journal homepage: www.elsevier.com/locate/agrformet

Evapotranspiration partitioning at the ecosystem scale using the stable isotope method—A review

Wei Xiao[a,*], Zhongwang Wei[b,c,**], Xuefa Wen[d]

[a] Yale-NUIST Center on Atmospheric Environment & Jiangsu Collaborative Innovation Center of Atmospheric Environment and Equipment Technology, Nanjing University of Information Science & Technology, Nanjing, China
[b] School of Forestry and Environmental Studies, Yale University, New Haven, United States
[c] River and Environmental Engineering Laboratory, Department of Civil Engineering, The University of Tokyo, Tokyo, Japan
[d] Key Laboratory of Ecosystem Network Observation and Modeling, Institute of Geographic Sciences and Natural Resources Research, Chinese Academy of Sciences, Beijing, China

ARTICLE INFO

Keywords:
Evapotranspiration partitioning
Stable isotope
Two-source mixing model
Craig-Gordon model
Keeling plot approach
Kinetic fractionation factor

ABSTRACT

Terrestrial evapotranspiration (*ET*) consists of evaporation (*E*) from canopy-intercepted water, evaporation from soil and open water, and transpiration (*T*) from plants. Determining the contribution of *T* to *ET* (hereafter *T*/*ET*) is challenging but necessary for improving water resource management and understanding the response of ecosystem water/energy budgets to climate change. Water stable isotopes provide unique information on ecosystem processes and can be used to partition evapotranspiration at the ecosystem scale. In this paper, the aim is to review the state of the science on the isotope method for ecosystem *ET* partitioning, with a focus on uncertainties related to estimating the three isotopic end members (isotopic compositions of *ET*, *T* and *E*). The published results show larger *T*/*ET* variations during the growing season in croplands due to water management and rapid leaf area index (LAI) changes compared to in other natural ecosystems. Another robust result is that on average, grasslands have lower *T*/*ET* than woodlands. The isotopic composition of *ET* is provided by measurements, while the isotopic compositions of *T* and *E* are generally obtained using the Craig-Gordon model with appropriate modifications. Significant advances have been made in the techniques for estimating the isotopic composition of *ET*, largely due to the availability of fast-responding instruments for in situ measurements of water vapor isotopic composition. The largest source of uncertainty in the *T*/*ET* estimation comes from uncertainties in the isotopic composition of *ET*. Based on published results of the uncertainties in the three end members, we estimate that a typical uncertainty range for *T*/*ET* is ± 21% (one standard deviation). This review provides background information and theoretical references for studies on isotopic hydrology, ecosystem processes and climate change.

1. Introduction

Terrestrial evapotranspiration (*ET*) refers to the amount of water vapor evaporated from the unit area of the land surface during a unit of time and consists of evaporation (*E*) from canopy-intercepted water, evaporation from soil and open water, and transpiration (*T*) from plants. Because the *T* process directly correlates with plant growth and the carbon cycle (Scott et al., 2006), quantitative estimation of *T* in the total evapotranspiration (*T*/*ET*) has long been acknowledged to play a crucial role in water resource management, yield estimation, the water cycle and climate change, from plot scale to global scale (e.g., Jasechko et al., 2013; Kool et al., 2014). For example, efforts to increase water use efficiency (the ratio of carbon gain to water loss) and control evaporative loss in agricultural land requires accurate determination of the consumption of water through plant activities. Because *T* fluxes link the water and carbon cycles, they are used to calculate carbon assimilation by terrestrial vegetation, so estimating *T* fluxes is a major focus in climate and ecology studies (Dubbert et al., 2014b; Jasechko et al., 2013; Jefferson et al., 2017). Therefore, the topic of evapotranspiration partitioning has gained much attention in the scientific community (e.g., Berkelhammer et al., 2016; Lu et al., 2017; Williams et al., 2004).

Various methods have been developed to partition *ET* at different time and spatial scales. At the global and regional scales, traditional methods are mostly model-related, such as satellite-based estimations

* Corresponding author.
** Corresponding author at: School of Forestry and Environmental Studies, Yale University, New Haven, United States.
E-mail addresses: wei.xiao@nuist.edu.cn (W. Xiao), zhongwang.wei@hydra.t.u-tokyo.ac.jp (Z. Wei).

https://doi.org/10.1016/j.agrformet.2018.09.005
Received 17 November 2017; Received in revised form 5 August 2018; Accepted 5 September 2018
Available online 15 September 2018
0168-1923/ © 2018 Elsevier B.V. All rights reserved.

(Martens et al., 2017; Miralles et al., 2011; Wei et al., 2017; Zhang et al., 2016), land surface models (e.g., Wang-Erlandsson et al., 2014), and reanalysis data (Chen et al., 2014; Kochendorfer and Ramírez, 2010). Isotopic measurements (Gibson and Edwards, 2002; Good et al., 2015; Jasechko et al., 2013) have also been used to partition *ET* at these scales. There is a considerable discrepancy among global *T/ET* estimated using different methods. For example, the results of a combination of widely ranging, remotely-sensed observations showed that approximately 80% of the annual land *ET* is attributed to *T* (Miralles et al., 2011). Wei et al. (2017) quantified the global *T/ET* with a leaf area index (LAI)-based *ET* partitioning algorithm and concluded that *T* accounts for 57% of *ET*. The distinct isotope effects of *T* and *E* based on the isotopic analysis of a global dataset of large lakes and rivers showed that *T* represents 80–90% of terrestrial *ET* (Jasechko et al., 2013), although this estimate was challenged by Coenders-Gerrits et al. (2014). The results of isotope mass budget-based simulations suggested that the transpired fraction of *ET* accounts for approximately 60% of the annual land *ET* (Good et al., 2015).

At the plot scale, *T/ET* can be quantified using isotopic measurements and a combination of traditional in situ measurements, such as those from eddy covariance systems, Bowen ratio systems, weighing lysimeters, sap-flow meters, leaf conductance upscaling, chamber measurements, and the concept of underlying water use efficiency (WUE). For example, Scanlon and Sahu (2008) and Scanlon and Kustas (2010) proposed utilizing carbon dioxide (CO_2) and water vapor ecosystem fluxes to determine *T/ET*. Combinations of the eddy covariance method with sap-flow and lysimeter-based techniques have also been widely applied (e.g., Kelliher et al., 1992; Kool et al., 2014). Zhou et al. (2016) and Scott and Biederman (2017) partitioned *T/ET* using the concept of ecosystem scale water use efficiency determined from eddy covariance *ET* and gross ecosystem photosynthesis. Good et al. (2014); Hu et al. (2014) and Wei et al. (2015) partitioned *ET* based on isotopic measurements. These methods are well documented in several recent reviews (e.g., Kool et al., 2014; Schlesinger and Jasechko, 2014; Sutanto et al., 2014; Zhang et al., 2010).

Although vastly important and widely studied, *ET* partitioning is still subject to great debate (e.g., Coenders-Gerrits et al., 2014; Jasechko et al., 2013; Schlaepfer et al., 2014; Schlesinger and Jasechko, 2014; Sutanto et al., 2014). At the plot scale, *T/ET* values estimated from scaled sap-flow can be 15% lower than those estimated by the isotope approach (Williams et al., 2004). Wei et al. (2018) also reported 10–20% *T/ET* differences between estimations using isotopes and estimations using a two-source *ET* model simulation.

Among the approaches cited above, isotopic methods accounting for different kinetic fractionation effects for transpiration and evaporation processes have been used for *ET* partitioning for the past twenty years (e.g., Dubbert et al., 2013, 2014b; Williams et al., 2004; Wu et al., 2017). The saturation vapor pressure and molecular diffusivities of the minor water molecules ($^1H_2{}^{18}O$ and $^1H^2H^{16}O$) are lower than those of the most abundant water molecule ($^1H_2{}^{16}O$) (Majoube, 1971; Merlivat et al., 1963; Merlivat, 1978; Cappa et al., 2003). During the evaporation process, the lighter water molecules easily leave the liquid evaporation surface (water, soil or leaf surface), while the heavier water molecules ($^1H_2{}^{18}O$ and $^1H^2H^{16}O$) accumulate at the surface. Therefore, soil water is more isotopically enriched at the evaporating surface than at other depths (Zimmermann et al., 1966). Plant water uptake does not cause fractionation, and transpiration can often be assumed to be in an isotopic steady-state or that its isotopic composition is the same as that of the xylem water. The difference in isotopic compositions between *E* and *T* forms the basis for *ET* partitioning using isotopic methods.

The isotopic approach has been widely used for *ET* partitioning at the ecosystem (e.g., Dubbert et al., 2013, 2014b; Wang and Yakir, 2000; Williams et al., 2004; Table 1), regional (Lee et al., 2010; Jasechko et al., 2013) and global scales (Good et al., 2015; Jasechko et al., 2013). However, *T/ET* estimations based on isotopic measurements, either at the global scale or at the ecosystem scale, are generally higher than the estimations based on conventional or non-isotopic experimental observations and land surface models (Schlesinger and Jasechko, 2014; Sutanto et al., 2014). Previous studies have suggested that the isotopic compositions of *E*, *T* and *ET*, which constitute the basis of this approach, obtain large errors (e.g., Griffis, 2013; Sutanto et al., 2014; Wu et al., 2017). Although these deficiencies have been addressed in many studies (e.g., Griffis, 2013; Sutanto et al., 2014; Wu et al., 2017), the effects of uncertainties in each component (*E*, *T* and *ET*) on *T/ET* estimation are still not well known. Nevertheless, the water stable isotopes are powerful tools for partitioning *ET* because these isotopes provide unique information regarding the water in the soil-vegetation-atmosphere continuum. The stable isotopic method for *ET* partitioning is usually based on the principle of isotopic mass balance; thus, the analysis of the water stable isotopic compositions within soil, vegetation and the atmosphere is the core issue.

In this paper, the aim is to review *ET* partitioning at the ecosystem scale using the isotopic method.

In Section 2, the mass conservation principles underpinning this method are described and an overview of the relevant publications on this topic are provided. The next three sections discuss methods and theories for estimation of the three ecosystem isotopic end members: isotopic composition of *ET* (δ_{ET}, Section 3), isotopic composition of evaporation (δ_E, Section 4) and isotopic composition of transpiration (δ_T, Section 5). In Section 6, uncertainties in *T/ET* associated with errors in these end members are presented. In Section 7, we briefly discuss potential sources of discrepancies between the isotopic method and other ecosystem partitioning methods. Special emphasis is given to the key concepts and processes presented in the schematic diagram shown in Fig. 1.

2. Isotope-based *ET* partitioning at the ecosystem scale: an overview

2.1. Mass balance consideration

The isotopic method for *ET* partitioning is based on two isotopic mass balance equations: one for $^1H_2{}^{16}O$ and one for either $^1H^2H^{16}O$ or $^1H_2{}^{18}O$. At the ecosystem scale, without considering canopy interception, the isotopic two-source mixing model is the most popular isotopic method for evapotranspiration partitioning (Table 1), although several studies are based on the soil water balance principle (i.e., Ferretti et al., 2003; Hsieh et al., 1998; Robertson and Gazis, 2006; Wenninger et al., 2010) and total isotopic budget balance approaches (Sutanto et al., 2012). In this two-source framework, ecosystem evapotranspiration consists of *T* and *E*:

$$ET = E + T \tag{1}$$

The components also obey the isotopic mass balance:

$$R_{ET}ET = R_E E + R_T T \tag{2}$$

where R_{ET}, R_E and R_T are the (either oxygen or hydrogen) stable isotopic molar ratios of ecosystem evapotranspiration, soil evaporation and plant transpiration, respectively. Converting notation "*R*" to "*δ*", Eq. (2) becomes the following:

$$\delta_{ET}ET = \delta_E E + \delta_T T \tag{3}$$

where δ_{ET}, δ_E and δ_T are the (either oxygen or hydrogen) stable isotopic compositions of ecosystem evapotranspiration, soil evaporation and plant transpiration, respectively, expressed as delta notation.

The *R* and *δ* notations are related to the water vapor fluxes (*ET*, *T* or *E*) in the following manner. Let F_x represent the molar flux of $^1H_2{}^{16}O$, and F_x' represent the molar flux of the minor isotopic water molecules ($^1H^2H^{16}O$ or $^1H_2{}^{18}O$). Their molar ratio R_x is as follows:

Table 1
Studies of evapotranspiration partitioning at the ecosystem scale using the stable isotopic two-source mixing model.

Continent	Country/Region	Ecosystem	Location	Period	isotope	δ_{ET}	δ_E	δ_T	Laser analyzer	References
Africa	Haouz plain, Morocco	Winter wheat	31°68′N, 7°38′W	5 d	^2H	Keeling	CG	δ_X	ICOS	Aouade et al. (2016)
	Marrakeck, Morocco	Olive orchard	–	4 d	^2H	Keeling	CG	δ_X	–	Williams et al. (2004)
	Niamey, Niger	Woody shrubs	13–14 °N, 2–3 °E	12 d	^2H	An isotopic mass balance model	CG	δ_X	–	Brunel et al. (1997)
	Laikipia Plateau, Kenya	Dry land grass patch	0.3229 °N, 36.9028 °E	10 d	^2H	Keeling	CG	Chamber	ICOS	Good et al. (2014)
Europe	Central Portugal	Oak-oak woodland	39°8′17.84″N, 8°20′3.76″W	5 d	^{18}O	Chamber	CG/Chamber	DN	CRDS	Dubbert et al. (2013)
	Central Portugal	Understory of an oak savanna	39°8′17.84″N, 8°20′3.76″W	26 d	^{18}O	Chamber	CG/Chamber	DN	CRDS	Dubbert et al. (2014b)
	INRA Lusignan, France	Perennial grass[1]	46°25′N, 0°6′W	5 d	^{18}O	Condensation	Water source	δ_X	–	Rothfuss et al. (2010)
	Negev, Israel	Agroforest system	–	5 d	^{18}O	Keeling	CG	δ_X	–	Wang and Yakir (2000)
North America	California, USA	Sorghum	38.867 °N, 115.448 °W	10 d	^2H, ^{18}O	Chamber	Chamber	Chamber	ICOS	Lu et al. (2017)
	Arizona, USA	Grassland	31°78′N, 100°88′W	15 d	^2H	Keeling	CG/Keeling	FC	–	Yepez et al. (2005)
	Arizona, USA	Semiarid savanna woodland	31°39′49″N, 110°10′39″W	1 d	^2H, ^{18}O	Keeling	CG	δ_X	–	Yepez et al. (2003)
	Arizona, USA	Semiarid savanna woodland	31°39′49″N, 110°10′39″W	5 d	^{18}O	Keeling	CG	DN	–	Yepez et al. (2007)
	Arizona, USA	Mesquite tree[2]	32°37.13′N, 110°47.05′W	–	^2H	Keeling	CG	Chamber	ICOS	Wang et al. (2010)
	Oklahoma, USA	Grassland[3]	34.982 °N, 97.521 °W	5 d	^2H	Chamber Keeling	CG/Chamber /Keeling	Chamber/soil water/ Keeling	ICOS	Wang et al. (2013)
	Colorado, USA	Forest	40.03 °N, 105.55 °W	Growing season	^{18}O	Keeling	CG	DN	CRDS	Berkelhammer et al. (2016)
	Connecticut, USA	Mixed forest	41°58′N, 73°14′W	–	^{18}O	CG	Precipitation	δ_X	TDL	Lee et al. (2007)
South America	Sonora, México	Semi-arid ecosystem	29.741 °N, 110.5337 °W	1 d	^{18}O	Keeling	CG	δ_X	–	Tarin et al. (2014)
	Paragominas, Brazil	Forest and pasture	2°59′S, 47°31′W	1 d	^2H, ^{18}O	Keeling	Flanagan	δ_X	–	Moreira et al. (1997)
	Manaus, Brazil	Forest & pasture	3°8′S, 60°1′W	1 d	^2H, ^{18}O	Keeling	Flanagan	δ_X	–	Moreira et al. (1997)
Asia	Eastern Mongolia	Grassland	47°13′N, 108°44′E	4 d	^{18}O	Keeling	CG	δ_s	–	Tsujimura et al. (2007)
	Eastern Mongolia	Forest	48°21′N, 108°39′E	5 d	^{18}O	Keeling	CG	δ_s	–	Tsujimura et al. (2007)
	Inner Mongolia, China	Grassland	42°02′N, 116°17′E	6 d	^{18}O	FG	CG	CG/FC/MBM	TDL	Hu et al. (2014)
	Luancheng, China	Wheat	37°53′N, 114°41′E	16 d	^{18}O	FG	CG	δ_X/FC	TDL	Wei et al. (2018)
	Luancheng, China	Corn	37°53′N, 114°41′E	13 d	^{18}O	FG	CG	δ_X/FC	TDL	Wei et al. (2018)
	Heihe, China	Oasis spring maize	38°51′N, 100°22′E	Growing season	^{18}O	FG	CG	MBM	CRDS	Wen et al. (2016)
	Gansu, China	Maize	37°52′N, 102°51′E	18 d	^{18}O	Keeling	CG/Chamber	Chamber	CRDS	Wu et al. (2017)
	North China	Forest	35°01′N, 112°28′E	3 d	^{18}O	Keeling	CG	FC	ICOS	Sun et al. (2014)
	Hebei, China	Winter wheat	37°53′N, 114°41′E	5 d	^{18}O	Keeling	CG	δ_X	TDL	Yuan et al. (2010)
	Hebei, China	Winter wheat	37°53′N, 114°41′E	2 d	^2H, ^{18}O	Keeling	CG	δ_X	–	Zhang et al. (2011)
	Wolong Nature Reserve, China	Subalpine Shrubland	30°51.437′N, 102°58.308′E	3 d	^2H, ^{18}O	Keeling	CG	δ_X	–	Xu et al. (2008)
	Tsukuba, Japan	Paddy field	36°03′14.3″N, 140°01′36.9″E	Growing season	^2H	Keeling	CG	Water source	CRDS	Wei et al. (2015)
	Tsukuba, Japan	Paddy field	36°03′14.3″N, 140°01′36.9″E	70 d	^{18}O	Keeling	CG	δ_X/FC	CRDS	Wei et al. (2018)
	Tsukuba, Japan	Lawn	36.1 °N, 140.1 °E	7 d	^2H, ^{18}O	Keeling	CG	δ_s	–	Yamanaka and Tsunakawa (2007)

Note: [1]Climate chamber; [2]Biosphere 2 greenhouse; [3]Climate-controlled experiment.
CG: Craig-Gordon model; DN: model of Dongmann et al. (1974); Flanagan: Eq. (5) of Flanagan et al. (1991); Keeling: Keeling plot approach; MBM: mass balance model; FC: Farquhar-Cernusak model.
ICOS: a water vapor isotope analyzer based on off-axis integrated cavity output spectroscopy (Los Gatos Research Inc., Mountain View, CA, USA). CRDS: a water vapor isotope analyzer based on cavity ring-down spectrometer (Picarro, Santa Clara, CA, USA). TDL: a tunable diode laser analyzer (Campbell Sci. Inc., Logan, UT, USA).

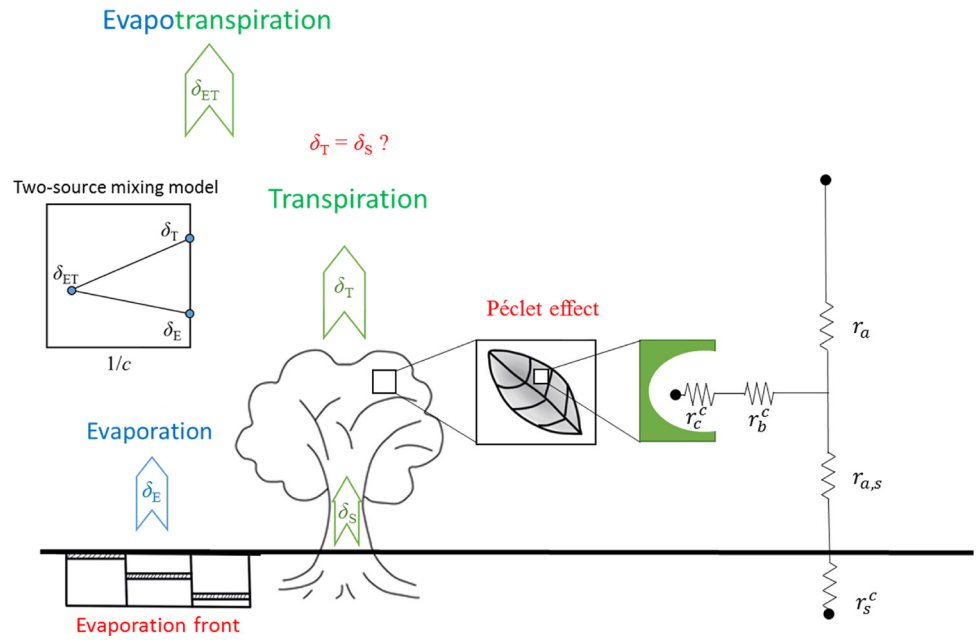

Fig. 1. Schematic diagram of the key points in the estimation of isotopic water vapor fluxes.

$$R_x = \frac{F_x'}{F_x} \tag{4}$$

The delta (δ) notation is used to represent the isotopic composition normalized in reference to an international standard (Coplen, 2011):

$$\delta_x = \left(\frac{R_x}{R_{VSMOW}} - 1\right) \tag{5}$$

where R_{VSMOW} is the $^2H/^1H$ or $^{18}O/^{16}O$ molar ratio of the Vienna Standard Mean Ocean Water (VSMOW), whose values are 0.00015576 and 0.0020052, respectively. By convention, the equation above is multiplied by 1000, so the unit of δ_x is ‰.

By incorporating Eq. (1) into (3), we obtain the ratio of T to ET (f_T):

$$f_T = \frac{T}{ET} = \frac{\delta_{ET} - \delta_E}{\delta_T - \delta_E} \tag{6}$$

This method is termed the isotopic two-source model. Implementation of this model requires that three isotopic end members (δ_{ET}, δ_E and δ_T) be known.

2.2. Literature review of isotope-based ET partitioning at the ecosystem scale

The T/ET ratios obtained with the stable isotopic two-source model at the ecosystem scale are summarized in Fig. 2. This summary includes a diverse range of ecosystems, such as cropland, grassland, woodland, and paddy fields in Africa, Europe, North America, Asia and Oceania. The f_T value ranges from 52% to 100% for cropland, from 43% to 100% for grassland, and from 61% to 100% for woodland. For paddy fields, f_T ranges from 20% in the early growing season to 100% in the late growing season.

Cropland is one of the most studied vegetation types. For wheat ecosystems, T is the major component of ET. For a mature wheat ecosystem in central Israel, soil evaporation contributes only 1.5–3.5% to ET at midday, while f_T exceeds 96.5% (Wang and Yakir, 2000). In northern China, the f_T of winter wheat during the growing season is relatively high (94.8–99.7%; Yuan et al., 2010), but the value is lower during the irrigation season (60–83%; Zhang et al., 2011). In a semiarid region, the peak value of f_T in a winter wheat field is relatively small; its value ranges from 59 to 73% during the rapid-growth season and from 77 to 83% before irrigation (Aouade et al., 2016). For a rice paddy in Japan, f_T is low during the early growing season but approaches a constant value of close to 1 during the late growing season, with an average uncertainty of 14 ± 10% (Wei et al., 2015). For a sorghum ecosystem in California, USA, f_T ranged from 39.3% to 52.3% during 24 July to 20 August 2014 with a standard deviation of 5.6% (Lu et al., 2017). The deployment of an isotopic laser spectrometer has made ET partitioning at a high temporal resolution possible; the diurnal variation in f_T is 71–96% (mean value of 87 ± 5.2%) for a summer maize in an oasis cropland (Wen et al., 2016). The f_T value in a maize field ranges from 52% to 91% during the entire growing season, and the uncertainty of the partitioning result ranges from 1.4% to 14.1% (Wu et al., 2017). Moreover, Wei et al. (2018) found that f_T in the growing season is 73 ± 5% for rice, 92 ± 1% for wheat (LAI > 2.5) and 82 ± 1% for corn, with seasonal ranges of 20–100%, 80–100% and 20–100%, respectively.

The ET partitioning of grassland ecosystems has also been studied. Moreira et al. (1997) suggested that transpiration is not a major source of water vapor above the grassy pastures in the Amazon basin. Yepez et al. (2005) showed that f_T of an *Eragrostis lehmanniana* grassland increases from 35 ± 7% to 43 ± 8% during the first 3 days after irrigation but decreases to 22 ± 5% on the seventh day. At a grassland site in eastern Mongolia, the f_T was 35–59% (Tsujimura et al., 2007). Transpiration from a lawn increased from ~75% in the first month of the growing season to more than 80% over the latter months, with a standard deviation of f_T ranging from 5% to 10% (Yamanaka and Tsunakawa, 2007). In a climate-controlled experiment, the diurnal variation in f_T over grassland in Inner Mongolia shows a "U" pattern: the f_T values decrease from 6:30–10:30, remained stable from 10:30–15:30 (value of 75%), and increase in the afternoon. The mean value of f_T during the time period of 6:30–18:30 across 6 days is 83%. The uncertainty of f_T estimation introduced by the uncertainty of δ_E and δ_{ET} are 2.8% and 21.4%, respectively (Hu et al., 2014). In a manipulative field experiment, Wang et al. (2013) reported that the f_T of a grassland ecosystem in Oklahoma, USA is 77 ± 15% under controlled conditions but increases to 86 ± 10% after a 2 °C temperature increase. In a dry land grass patch, the f_T ranges from 0% to 40% during the green-up phase and then decreases, with an average ratio of 29% and an average uncertainty of ~5% (Good et al., 2014). In a semiarid ecosystem in northwestern Mexico, the f_T decreases from 86 ± 21% in the morning to 46 ± 9% in the afternoon, with a mean value of

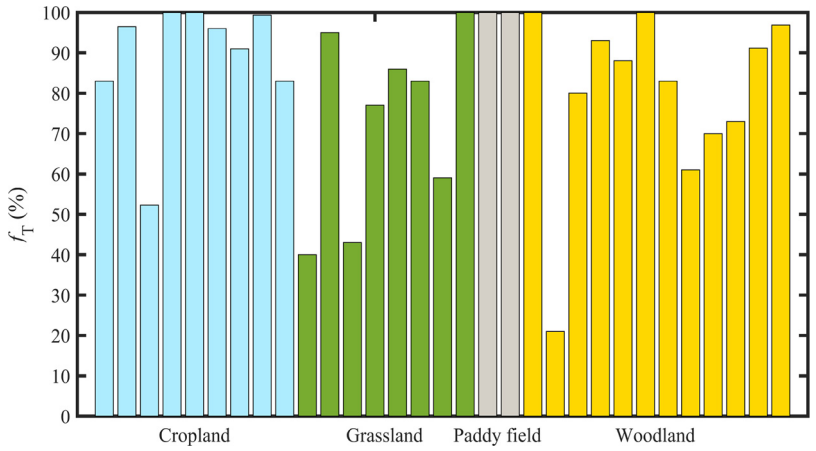

Fig. 2. Maximum f_T values in the literature; the values were reported using the stable isotopic two-source model at the ecosystem scale.

59 ± 6% (Tarin et al., 2014).

A number of researchers have investigated forest or shrub ecosystems and have shown that the *T* fraction varies significantly among ecosystem types and climatic conditions. Brunel et al. (1997) found that plant transpiration contributes approximately 20% of the total evapotranspiration in an area of fallow bushland of woody shrubs. Moreira et al. (1997) proposed that transpiration is responsible for most of the evapotranspiration in the Amazon rainforest during the dry season. In an olive orchard in Morocco, the f_T is 100% prior to irrigation and falls between 69% and 86% after irrigation (Williams et al., 2004). In a semiarid riparian woodland, the f_T is 90% for the entire growing season, with a low value of 65% during wet conditions and a high value of 100% during dry conditions, and the standard deviation of f_T ranges from 3% to 15% (Yepez et al., 2007). At a forest site in eastern Mongolia, the f_T was 60–73% (Tsujimura et al., 2007). In the Wolong Nature Reserve of China, the f_T values of a subalpine shrubland during a three-day time period in the early monsoon season are 74.5 ± 9.9%, 65.6 ± 8.3% to 96.9 ± 2.0% (Xu et al., 2008). Yepez et al. (2003) reported that in a semiarid savanna woodland in southeastern Arizona, USA the f_T value is 85 ± 6% during the post-monsoon period, while the *T* fraction of the grass layer constitutes approximately 50% of the understory *ET*. The f_T value of a savanna-oak woodland in central Portugal ranges from 20% to 80% (Dubbert et al., 2013). The contribution of understory vegetation to *ET* in a cork-oak woodland in central Portugal reaches 43% (Dubbert et al., 2014b). The *T* fractions of two needleleaf forested sites in the USA are 62 ± 27% and 49 ± 23% (Berkelhammer et al., 2016). The diurnal variation in f_T of a *Quercus variabilis* oak woodland in northern China indicated that the value increases in the morning, peaks (91.19 ± 4.86%, 86.30 ± 3.52% and 85.37 ± 6.87%) from 10:00–14:00 and decreases to less than 60% from 16:00–18:00 (Sun et al., 2014). Lee et al. (2007) estimated that the transpiration of the overstory trees contributes 70% to the whole-stand transpiration in a temperate forest.

In addition to studies under natural conditions, *ET* partitioning experiments under controlled conditions have also been conducted. In the Biosphere 2 greenhouse, the f_T value increases as woody plant cover increases; values of 61% and 83% for 25% and full plant cover, respectively, were recorded (Wang et al., 2010). Under fully controlled conditions in a climate chamber, the *T* fraction increases gradually as plant growth increases; f_T is 0 for bare soil but increases to 6% (with uncertainty of 2%) on the sixteenth day after seeding and to 95% (with uncertainty of 48–74%) after 43 days (Rothfuss et al., 2010).

Several broad generalizations can be made from the data shown in Fig. 2 and the literature reviewed above. (1) Some of the variations in the observed *T/ET* can be explained by a balance between water supply and atmospheric evaporative demand (Good et al., 2017). An example of this balance is the reduction of cropland *T/ET* in response to irrigation. (2) Cropland systems (both dryland crops and rice paddies) seem to show larger *T/ET* variations during the growing season than other natural ecosystems due to water management and rapid LAI changes. (3) On average, grasslands have lower *T/ET* than woodlands.

3. Estimation of the isotopic composition of evapotranspiration

3.1. Measurement of isotopic flux

3.1.1. Chamber method for isotopic flux

The methods used in studies for observing δ_{ET}, δ_E and δ_T in *ET* partitioning are shown in Table 1. In situ and continuous measurements of the isotopic composition of water vapor are possible with stable isotopic laser spectrum techniques. Chamber methods have been combined with the use of laser analyzers (such as the water vapor isotope analyzers based on cavity ring-down spectrometer and off-axis integrated cavity output spectroscopy, Table 1) to observe δ_E, δ_T and δ_{ET} (Lu et al., 2017; Wang et al., 2012, 2013). In these studies, transparent acrylic chambers that contain a fan are connected to an isotopic water vapor analyzer. A relatively small chamber is used to measure δ_T, and larger chambers are used to measure bare soil or combinations of soil and plants. The experiments cited here were performed under adequate sunshine.

The isotopic composition of water vapor flux (δ_F) can be calculated as follows:

$$\delta_F = \frac{C_M\delta_M - C_V\delta_V}{C_M - C_A} \tag{7}$$

where δ_F can be δ_E, δ_T or δ_{ET}, C_V and C_M represent the water vapor concentration of the ambient atmosphere and the air inside the chamber, respectively, and δ_V and δ_M are the isotopic compositions of the water vapor outside and inside the chamber, respectively. The chamber approach was also used to measure the isotopic compositions of *T* (Dubbert et al., 2017) and *E* (Dubbert et al., 2013, 2014a, b; Lu et al., 2017; Wang et al., 2013; Wu et al., 2017).

3.1.2. Eddy covariance isotopic flux method

High-frequency isotope measurements from laser-based analyzers have also been combined with the eddy covariance method to estimate δ_{ET} (Good et al., 2012; Griffis et al., 2008, 2010):

$$\delta_{ET} = \frac{\overline{\chi_V}}{\overline{w'\chi_V'}}\overline{w'\delta_V'} + \overline{\delta_V} \tag{8}$$

where χ_V is the molar mixing ratio of water vapor (moles of water molecules in 1 mol dry air, mol mol^{-1}), $\overline{w'\chi_V'}$ is the covariance of the vertical wind velocity *w* and χ_V, δ_V is the isotopic composition of the atmospheric water vapor, and $\overline{w'\delta_V'}$ is the isoforcing (‰ m s^{-1}) (Lee

et al., 2009). However, this approach can introduce many uncertainties due to the loss of information inherent to the measured items when calculating the covariance between isotopic compositions and vertical wind fluctuations (Good et al., 2012).

3.2. Keeling plot approach

The Keeling plot method (Keeling, 1958; Yakir and Sternberg, 2000) is the most popular method for estimating δ_{ET} and δ_E. Of the 33 studies surveyed in Table 1, 23 applied the Keeling plot approach. In this approach, the atmospheric water vapor concentration, C_V, is the sum of the background atmospheric water vapor concentration C_{bg} and the water vapor contributed by the ecosystem evapotranspiration C_{ET}:

$$C_V = C_{bg} + C_{ET} \tag{9}$$

Similarly, for water stable isotopes, the mass balance principle is as follows:

$$C_V\delta_V = C_{bg}\delta_{bg} + C_{ET}\delta_{ET} \tag{10}$$

where δ_V, δ_{bg} and δ_{ET} are the isotopic compositions of the actual atmosphere, background atmosphere and ecosystem evapotranspiration, respectively. By combining Eqs. (9) and (10) and converting water vapor concentration to water vapor mixing ratios based on the relationship $C_{bg}/C_v = \chi_{bg}/\chi_v$, we obtain the following:

$$\delta_V = \chi_{bg}(\delta_{bg} - \delta_{ET})(1/\chi_V) + \delta_{ET} \tag{11}$$

This equation shows the linear relationship between δ_V and $(1/\chi_V)$ with a slope of $\chi_{bg}(\delta_{bg}- \delta_{ET})$ and an intercept of δ_{ET}. Therefore, if χ_V and δ_V are observed, δ_{ET} can be obtained through linear regression. The Keeling plot method is widely used to estimate δ_{ET} (e.g., Aouade et al., 2016; Wang et al., 2010; Williams et al., 2004).

The regression can be conducted using both spatial and temporal gradients. Until high temporal resolution and continuous observations of isotopic water vapor were available, non-continuous observations of χ_V and δ_V were made at different heights for the linear regression of the Keeling plot approach (Lu et al., 2017; Wang and Yakir, 2000; Wang et al., 2010; Williams et al., 2004; Xu et al., 2008; Yepez et al., 2003). The development of the isotopic laser spectrum analyzer has allowed for continuous observations to use in Keeling plot analyses (Berkelhammer et al., 2016; Sun et al., 2014; Wang et al., 2013; Wei et al., 2015; Yuan et al., 2010; Zhang et al., 2011).

3.3. Flux-gradient method

As a micrometeorological method, the flux-gradient method measures δ_{ET} or δ_E without changing the ambient environment above the ground surface (Lee et al., 2007). Based on the flux-gradient relationship, the water vapor flux can be calculated from the water vapor concentration gradient between two heights and the eddy diffusivity K ($m^2\ s^{-1}$) (Baldocchi et al., 1988; Lee, 2018). For the water vapor flux of $^1H_2{}^{16}O$ (F_{ET}), the expression is as follows:

$$F_{ET} = -\frac{K}{M_V}\frac{\Delta C}{\Delta z} \tag{12}$$

where Δz is the height difference, ΔC is the difference in the water vapor concentration between the two heights and M_V is the molar mass of $^1H_2{}^{16}O$.

It is assumed that the eddy diffusivities (K) for all the water vapor isotopes ($^1H_2{}^{18}O$, $^1H^2H^{16}O$ and $^1H_2{}^{16}O$) are equal (Griffis et al., 2005; Lee et al., 2007; Yakir and Wang, 1996). For $^1H_2{}^{18}O$ or $^1H^2H^{16}O$, the evapotranspiration F'_{ET} is given by a formula similar to Eq. (12):

$$F'_{ET} = -\frac{K}{M'_V}\frac{\Delta C'}{\Delta z} \tag{13}$$

where $\Delta C'$ is the molar difference between the two heights and M'_V is the molar mass of $^1H_2{}^{18}O$ (or $^1H^2H^{16}O$). Therefore, the ^{18}O (or ^2H) composition of evapotranspiration is as follows:

$$R_{ET} = \frac{F'_{ET}}{F_{ET}} = \frac{\Delta C'}{\Delta C} \tag{14}$$

According to Eq. (14), the isotopic composition of evapotranspiration can be calculated if the isotopic compositions of water vapor are measured at two heights. Considering $\Delta C'/C = \Delta\chi'/\Delta\chi$, the $^{18}O/^{16}O$ (or $^2H/^1H$) molar ratio of evapotranspiration can be calculated as follows:

$$R_{ET} = \frac{\hat{\chi}'_{a,2} - \hat{\chi}'_{a,1}}{\hat{\chi}_{a,2} - \hat{\chi}_{a,1}} \tag{15}$$

where $\hat{\chi}_{a,1}$ and $\hat{\chi}'_{a,1}$ represent the true values of the molar mixing ratio of $^1H_2{}^{16}O$ and $^1H_2{}^{18}O$ (or $^1H^2H^{16}O$) at height 1, respectively, and $\hat{\chi}_{a,2}$ and $\hat{\chi}'_{a,2}$ represent those respective values at height 2.

Because the isotopic water vapor mixing ratio measured directly using the isotopic water vapor laser analyzer is not an accurate value, calibration is necessary to obtain the accurate isotope composition.

If the experiment is conducted over bare soil, the isotopic composition of soil evaporation can be calculated using a similar method.

The application of the flux-gradient method for the in situ measurement of isotopic water vapor fluxes was first proposed by Lee et al. (2007). The method has subsequently been used in studies of *ET* partitioning (Hu et al., 2014; Wen et al., 2012, 2016) and the kinetic fractionation of open water evaporation (Xiao et al., 2017). Because the temporal resolution of the flux-gradient method is high (less than hourly), the temporal dynamics of δ_{ET} can be observed.

3.4. Uncertainties in δ_{ET} estimations

The disadvantages of the chamber method include the following: (1) the environmental conditions (such as wind speed and temperature) can change within the chamber; (2) the installation and maintenance of the chamber under natural conditions are difficult (Wei et al., 2015); and (3) leaf scale measurements must be scaled up for canopy-level estimations (Wu et al., 2017). Compared with the Keeling plot and the flux-gradient approaches, the eddy covariance approach is associated with significantly larger uncertainty due to the loss of information during the covariance calculation between the isotopic compositions and vertical wind fluctuations (Good et al., 2012; Sturm et al., 2012). The eddy covariance method is also used to measure δ_{ET} (e.g., Good et al., 2012, 2014; Griffis, 2013; Griffis et al., 2010) and will hopefully become important with the arrival of lasers on the market allowing for fast measurement (> 2 Hz). However, the discussion hereafter focuses on the potential uncertainties in the Keeling plot and gradient approaches.

Potential uncertainties exist in the assumptions of the Keeling plot approach. First, it is assumed that only two sources of atmospheric water vapor exist in the framework of the Keeling plot approach, i.e., water vapor from the ecosystem evapotranspiration and water vapor in the atmospheric background. The second assumption is that the temporal variations in the water vapor mixing ratio and δ_V are caused only by *ET*. However, the variation in δ_V at hourly or daily time scales is influenced mainly by the advection of air masses rather than by evapotranspiration (Lee et al., 2006), and the entrainment process by which air in the free atmosphere is moved downward and mixed with the atmospheric boundary layer also introduces biases in the Keeling plot estimates (Lee et al., 2012). Third, to obtain a slope value with a low standard error, C_{bg} (background atmospheric water vapor concentration), δ_{bg} (the isotopic composition of the background atmospheric water vapor) and δ_{ET} should be constant during the time interval of the regression (Lee et al., 2006; Wen et al., 2012). Under ideal conditions, when the variation in δ_V is controlled only by *ET*, the parameters C_{bg} and δ_{bg} can still vary significantly over a short time

interval (Lee et al., 2006). Fourth, the C_V and δ_V measurements at different heights are used for the linear regression of the Keeling plot approach in some studies (Good et al., 2012; Lu et al., 2017; Wang and Yakir, 2000; Wang et al., 2010; Williams et al., 2004; Xu et al., 2008; Yepez et al., 2003), but the result is sensitive to the data processing methods in terms of the average types of data used in the regression (Good et al., 2012). All the above assumptions influence the accuracy of the Keeling plot method. Thus, the results of *ET* partitioning based on the Keeling plot method will be uncertain. The estimation of δ_{ET} may be reliable at short time intervals, such as half an hour (Good et al., 2012).

Theoretically, the flux-gradient method is likely more accurate, as it does not require the severe assumptions involved in the Keeling plot analysis. Using a trace gas analyzer (with a frequency of 1 Hz) deployed in a cropland, Huang and Wen (2014) reported that the $\delta^{18}O$ of the *ET* derived from flux-gradient measurements has an average uncertainty of 4.6‰. The same system had an uncertainty of 7.9‰ for $\delta^{18}O_{ET}$ when used in a low flux environment (a temperate grassland in semiarid Inner Mongolia, China; Hu et al., 2014). A laboratory test of a similar high-frequency analyzer reveals a precision of 1.4‰ for the $\delta^{18}O$ of *ET* (Lee et al., 2007). Using the flux-gradient method in combination with a water vapor isotope analyzer, the average uncertainties are 11.2‰ for $\delta^{2}H_{ET}$ and 4.6‰ for $\delta^{18}O_{ET}$ over an arid artificial oasis cropland (Huang and Wen, 2014).

On the other hand, disadvantages remain for the flux-gradient method: (1) An analyzer with both high precision and a fast response time is required to ensure that the same air mass can be observed by two intakes; (2) bias at night is high due to a low water vapor gradient, but fortunately, uncertainties in the partitioning *ET* at night are not important for longer-term (days or longer) averages; (3) the measurement height should be located just above the canopy to ensure that the water vapor mixing ratio gradient and its variation are driven only by *ET* and are not affected by advection; and (4) potential uncertainties may arise from instrument precision, meteorological variables, footprint issues and the method used to calculate hourly values (Good et al., 2012).

Both discrepancy and agreement have been reported in previous studies between the Keeling plot and flux-gradient methods. Discrepancies between these two methodologies (Griffis et al., 2007; Lee et al., 2006, 2012) may be due to different water vapor flux footprints or variable atmospheric conditions. However, agreement between the Keeling plot and flux-gradient results has also been reported (e.g., Good et al., 2012; Griffis et al., 2004, 2005). Nearly identical values of δ_{ET} and its statistical uncertainty have been reported for the Keeling plot and flux-gradient methods over 30 min periods (Good et al., 2012).

Here, we use isotope measurement data from Lake Taihu sites in China (Xiao et al., 2017) to compare these two approaches for estimating $\delta^{2}H_{ET}$ (Fig. 3). Overall, the values obtained with the Keeling plot (using geometric mean regression) and the flux-gradient methods are highly correlated ($R^2 = 0.9$), although the values from the Keeling plot method are approximately 10‰ higher than those from the flux-gradient method. Similarly, Wei et al. (2018) reported that during midday periods, the results of both methods are highly correlated for the $\delta^{18}O_{ET}$ of a cropland ecosystem, but compared with the flux-gradient method, the Keeling plot method is biased low by 2.2‰. Good et al. (2012) also reported that the two methods perform similarly over 30 min periods. Nevertheless, because both approaches have their own limitations, their applications to partitioning studies should be used with caution. When choosing between the methods, it is important that inherent assumptions that affect model accuracy be satisfied.

4. Estimation of the isotopic composition of soil evaporation

4.1. Craig-Gordon model

The Craig-Gordon model is the most common method used for estimating the isotopic composition of soil evaporation (Craig and Gordon, 1965). Using the isotopic composition of soil water at the evaporating surface (δ_L) and atmospheric water vapor (δ_V) as well as various meteorological variables, the isotopic composition of evaporation (δ_E) can be calculated as follows:

$$\delta_E = \frac{\alpha_{eq}^{-1}\delta_L - h\delta_V - \varepsilon_{eq} - (1-h)\varepsilon_k}{1 - h + 10^{-3}(1-h)\varepsilon_k} \quad (16)$$

where α_{eq} (> 1) is the equilibrium fractionation factor calculated as a function of water surface temperature (Majoube, 1971), ε_{eq} is equal to $(1 - 1/\alpha_{eq}) \times 10^3$ (‰), ε_k is the kinetic fractionation, and h is the atmospheric relative humidity in reference to the surface water temperature.

The Craig-Gordon model was first proposed for calculating the isotopic composition of open water body evaporation. Zimmermann et al. (1967) reported that the model can be used to estimate the δ_E of saturated soil in the isotopic steady-state. Barnes and Allison (1983) used the model for unsaturated soil under both isothermal and steady-state conditions. Moreover, numerical models can also simulate δ_E under non-saturated and non-isothermal conditions (e.g., Braud et al., 2005). Because numerical models have not been used in the two-source mixing model for *ET* partitioning, further discussion on these models is omitted here.

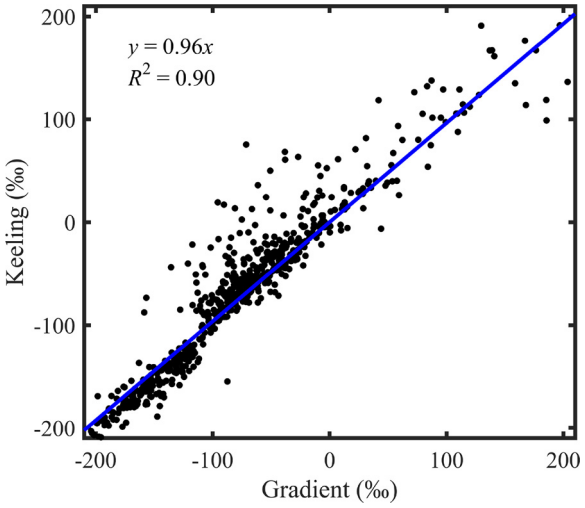

Fig. 3. Comparison of $\delta^{2}H_E$ values calculated using the flux-gradient method and the Keeling plot method based on isotope measurement data from Lake Taihu in China (Xiao et al., 2017) (only data points within the -200‰ to 200‰ range are shown).

4.2. Potential uncertainty in δ_E estimations

4.2.1. Isotopic composition of soil water at the evaporation front

The identification of the location and isotopic composition of the soil evaporation surface is vital for accurate estimations of δ_E (Fig. 1). Soil evaporation occurs at the interface between water vapor and liquid water, which is called the “evaporation front” (Braud et al., 2005; van de Griend and Owe, 1994; Wythers et al., 1999; Yamanaka and Yonetani, 1999). If the soil is saturated, evaporation occurs at the soil surface. If soil is not saturated, evaporation occurs at some depth in the soil. According to Barnes and Allison (1988), the evaporation front is located at a depth of 0.1–0.5 m in dry soils. Beneath the evaporation front, the isotopic composition decreases exponentially with increasing depth (Allison and Barnes, 1983; Walker and Brunel, 1990; Zimmermann et al., 1966, 1967). The location of evaporation fronts is influenced by meteorological conditions, soil water content and soil texture (Zimmermann et al., 1967). The evaporation fractionation generally occurs at deeper depths (0.5–3 m in depth) in arid and

Mediterranean climates and at shallower depths (0.2 to 0.3 m in depth) in temperate and tropical climates (Sprenger et al., 2016). Readers should be reminded that lateral heterogeneity in soil water isotopic composition profiles may exist, and these localized measurements are only meaningful if the profiles can be replicated in space.

In studies on *ET* partitioning, various methods have been used to determine the location of the evaporation front and its isotopic composition. The simplest method is to assume that the isotopic composition of surface soil water can represent δ_L. Xu et al. (2008) collected soil samples at depths of 1–10 cm, Wang et al. (2013) collected samples at depths of 0–2 cm, and Wu et al. (2017) collected samples at depths of 0–5 cm and 5–10 cm. The isotopic composition at the evaporation front is very sensitive to both the sampling depth and vertical profile of the soil water isotopic composition (Braud et al., 2009a, b). Using the Craig-Gordon model in conjunction with a climate chamber-controlled experiment, Rothfuss et al. (2010) showed that δ_L values derived from δ_E observations are 1–6‰ higher than the δ values of the soil water within the 1-cm surface layer, suggesting that sampling at the surface may cause biases.

Some researchers measured the vertical profile of the soil water isotopic composition at fine increments using the depth with a maximum value δ as the evaporation front position (Aouade et al., 2016; Dubbert et al., 2013, 2014b; Yepez et al., 2005; Yuan et al., 2010; Zhang et al., 2011). Yepez et al. (2005) reported that the mean isotopic composition in the 0–10-cm layer can represent δ_L on the first and third days after irrigation, while that in the 10–20-cm layer can represent δ_L at other times. Dubbert et al. (2013, 2014b) reported that the evaporation front is located at the soil surface when the soil is wet but decreases to approximately 2 cm as the soil water content decreases; in their studies, the variation in the δ value from 0 to 60 cm is 4.5‰ in the vegetation plots and 2.5‰ in the root and soil plots. Because δ_E is linearly correlated with δ_L with a coefficient (α_{eq}) close to 1, an accurate representation of δ_L is important for the estimation of δ_E. In addition to the methods that consider the depth of the maximum soil water isotopic composition as the evaporation front, Rothfuss et al. (2015) proposed identifying the evaporation front in the soil from the computation of soil water isotopic gradients.

To help the reader appreciate the vertical variation in the soil water isotopic compositions, in Fig. 4, we plot vertical profiles of the soil water isotopic compositions measured in the Qianyanzhou forest in China from July 21, 2011 to January 2, 2012 (Yang et al., 2015). Soil samples were collected at 20 depths at 5-cm increments from 5 cm to 100 cm. The mean $\delta^{18}O_s$ of this period indicates that the soil water in the relatively deeper layers (from 80 to 100 cm depth) and in the surface layers (from 5 to 20 cm depth) is more isotopically enriched than the soil water in the middle layers. Furthermore, the vertical profile varied on different days. For example, the soil water $\delta^{18}O_s$ gradually decreased from the deep layers to the topsoil on July 21, 2011, but significant enrichment in the surface layers was observed on October 9, 2011. Temporal variability in the vertical profiles indicates clear seasonal changes in the location of the evaporation front, emphasizing that detailed measurements are necessary for accurate *ET* partitioning.

Sensitivity analysis of δ_E can be conducted in a straightforward manner based on Eq. (16) and δ_s measurements. According to the measurement at the Qianyanzhou station on October 9, 2011, $\delta^{18}O_s$ in the upper 30 cm varied from −7.9‰ to −5.7‰, with a range of 2.2‰. If a typical value of relative humidity (h) is set to 0.7 and α_{eq} is close to 1, the variation in δ_E is approximately 7.3‰. Due to the significant sensitivity of δ_E to δ_s, the importance of accurate estimation for δ_s is evident. Moreover, if the δ_s values measured at 5, 20 and 45-cm depths are used, the δ_E can change by 19‰ to 41‰ in the afternoon (Fig. 5). The results highlight the importance of accurate isotopic value estimation at the evaporation front.

4.2.2. Soil kinetic fractionation factor

Estimation of the soil kinetic fractionation has long been a subject of debate (Braud et al., 2005, 2009a, b; Cappa et al., 2003; Luz et al., 2009; Rothfuss et al., 2012). Often for convenience, a constant value is used. For example, 26‰ and 13‰ were used by Williams et al. (2004) for the soil ε_k for $^1H^2H^{16}O$ before and after irrigation, respectively. The effect of turbulence was considered by Wang et al. (2010); their soil ε_k values are 16.4‰ and 10.9‰ without and with turbulence, respectively. A constant kinetic fractionation may not cause a large bias if the soil water content does not change considerably. Furthermore, the soil kinetic fractionation can be parameterized using formulas such as those for soil resistance, soil boundary layer resistance (i.e., Aouade et al., 2016) and aerodynamic resistance (i.e., Berkelhammer et al., 2016) (Fig. 1).

If the magnitude of the soil moisture variation is large, the effect of soil moisture on the kinetic fractionation factor should be considered (Dubbert et al., 2013). If the isotopic fractionation (α_k) of soil is affected only by molecular diffusion (Barnes and Allison, 1983), then

$$\alpha_k = D_v / D_v^i \tag{17}$$

where D_v is the molecular diffusivity of $^1H_2{}^{16}O$, and D_v^i is the molecular diffusivity of $^1H_2{}^{18}O$ or $^1H^2H^{16}O$.

To consider the effects of soil moisture and air turbulence, the equation should be modified as follows:

$$\alpha_k = \left(\frac{D_v}{D_v^i}\right)^n \tag{18}$$

where n represents the effects of air turbulence and molecular diffusion, and it can also be formulated as a function of soil moisture (Mathieu and Bariac, 1996), as in the following:

$$n = \frac{(\theta_{surf} - \theta_r)n_a + (\theta_{sat} - \theta_{surf})n_s}{(\theta_{sat} - \theta_r)} \tag{19}$$

where θ_{surf}, θ_{sat} and θ_r are the water contents of the soil surface, saturated and residual volumetric water content, respectively; $n = n_a$ for saturated soil and $n = n_s$ when soil surface water is minimum and in equilibrium with the atmosphere, with values of $n_a = 0.67$ and $n_s = 1$ for soil drying under a laminar air flow.

5. Estimation of the isotopic composition of plant transpiration

For the estimation of δ_T, three aspects have long been debated (Fig. 1): (1) Are the isotopic compositions of water entering (i.e., source water, δ_X) and exiting (δ_T) the leaves equal or not (i.e., isotopic steady-state versus non-steady-state assumptions, Section 5.1 and 5.2)? (2) Is the leaf water thoroughly mixed and uniformly distributed or not (i.e., Péclet effect, Section 5.3)? (3) How should the canopy kinetic fractionation factor be parameterized (Section 5.4)? These three problems will be discussed in the following sections. Furthermore, the water mass balance method for calculating δ_T (Section 5.5) and uncertainty in δ_T estimations (Section 5.6) will be discussed.

5.1. Steady-state assumption

For the estimation of δ_T, the simplest method is to assume that δ_T is equal to the isotopic composition of the source water (Fig. 1). In studies of stable isotope ecology, it is typically assumed that leaves are very thin, leaf water turnover is quick, and the isotope is uniformly distributed. Under such assumptions, the water mass of T is much higher than that of the leaf water; thus, the isotopic composition of water exiting the leaves is equal to that entering the leaves, i.e., $\delta_T = \delta_X$, a condition referred to as the isotopic steady-state (Farris and Strain, 1978; Forstel, 1978). On the basis of this assumption, we can obtain δ_T by measuring the isotopic composition of stem or twig water, and *ET* partitioning studies typically use measurements of this water (e.g., Aouade et al., 2016; Lee et al., 2007; Wang and Yakir, 2000; Williams et al., 2004; Xu et al., 2008; Yepez et al., 2003; Zhang et al., 2011).

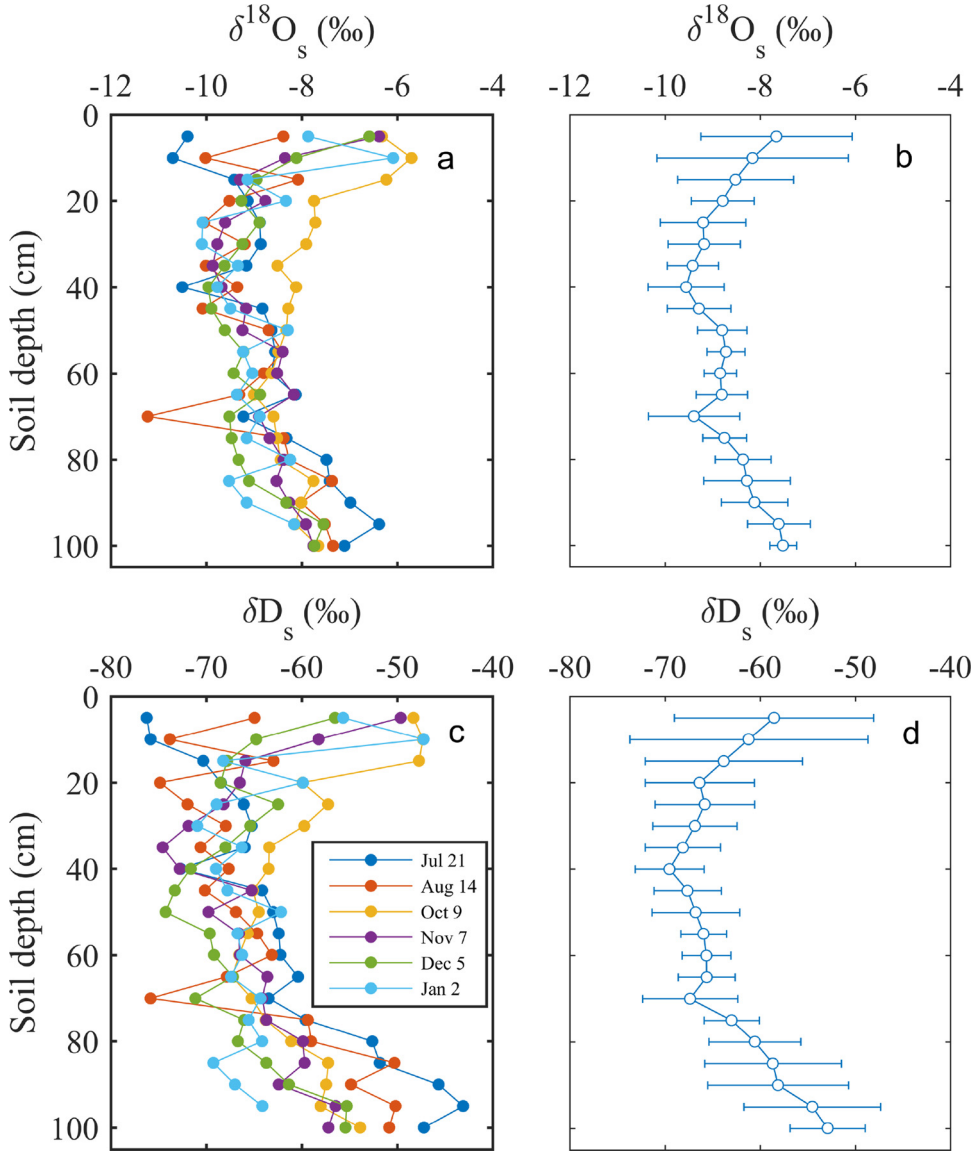

Fig. 4. Vertical profiles of the soil water isotopic compositions at the Qianyanzhou forest site from July 21, 2011 to January 2, 2012 (Yang et al., 2015).

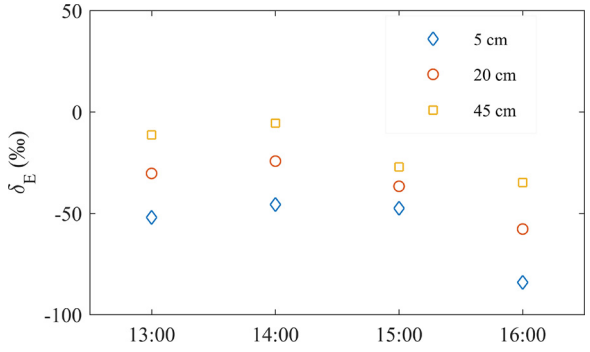

Fig. 5. $\delta^{18}O_E$ values calculated using soil isotopes at different depths.

5.2. Non-steady-state effects

Many observation and modeling studies have suggested that a steady-state occurs only during a short period (hourly) near midday or in shorter canopies (Flanagan et al., 1993). During rapidly changing environmental conditions or when the water vapor flux is very small, it is difficult for canopies to reach a steady-state (Cernusak et al., 2005; Dongmann et al., 1974; Farquhar and Cernusak, 2005; Lai et al., 2006; Welp et al., 2008; Xiao et al., 2012), and *ET* partitioning is affected by the short-term variations in δ_T (Dubbert et al., 2014b). Therefore, isotopic models that consider non-steady-state effects developed by Dongmann et al. (1974) and Farquhar and Cernusak (2005) are used to improve the δ_T calculation (Berkelhammer et al., 2016; Dubbert et al., 2013, 2014b; Hu et al., 2014; Sun et al., 2014; Yepez et al., 2005).

5.3. The Péclet effect

Using the steady-state assumption, we can derive the isotopic composition of leaf water using the Craig-Gordon model by assuming $\delta_T = \delta_X$ (δ_E in Eq. (16) should be δ_T if transpiration is considered). However, the derived δ_L is always higher than the observed values, which suggests that the leaf water is not thoroughly mixed. During the *T* process, the isotopic composition of the leaf water at the evaporation site in the stomata is the highest among all sites. Furthermore, stem xylem water is transferred continuously to leaves and dilutes the isotopic composition of the bulk leaf water. Therefore, a gradual decrease from the evaporation sites to leaf veins occurs, a phenomenon known as the Péclet effect (Fig. 1; Farquhar and Lloyd, 1993). Many experimental studies have confirmed the existence of the Péclet effect, such as those

by Cernusak et al. (2005); Farquhar et al. (2007) and Xiao et al. (2012). The Péclet model proposed by Farquhar and Lloyd (1993) is a one-dimensional advection-diffusion model; the results of this model are in close agreement with the empirical results. In addition, two-pool and string-of-lake models have been proposed to represent the distribution of leaf water isotopes (Gat and Bowser, 1991; Leaney et al., 1985). Omission of the Péclet effect will cause biases in the δ_T calculation (Farquhar and Cernusak, 2005).

Several researchers have observed isotopic fractionation during plant water uptake for some plants (Ellsworth and Williams, 2007; Vargas et al., 2017). As a result, δ_X may have different values for different parts of the stem. The manner in which this phenomenon alters the estimates of δ_T and *T/ET* remains unclear at the current stage and requires further investigation.

5.4. Kinetic fractionation effect

The kinetic fractionation effect controls the isotopic enrichment during *T*. At the leaf scale, this effect is formulated as a function of stomatal resistance and boundary layer resistance (Dongmann et al., 1974; Farquhar and Lloyd, 1993; Flanagan et al., 1991). At the canopy scale, a debate exists on how to consider the effect of turbulence (Fig. 1; Cuntz et al., 2003; Dongmann et al., 1974; Farquhar and Lloyd, 1993; Hoffmann et al., 2004; Lee et al., 2009; Xiao et al., 2010, 2012). Because air turbulence does not cause isotopic fractionation, it is reasonable to assume that increased air turbulence must weaken kinetic fractionation. However, Lee et al. (2009) reported the opposite conclusion: air turbulence can enhance kinetic fractionation rather than weaken it in terrestrial environments because gaseous diffusion dominates the stomatal pathway when air turbulence is strong. In the calculation of canopy scale kinetic fractionation, aerodynamic resistance should be included in the denominator of the equation that expresses the overall kinetic effect as a weighted mean value of the contributions associated with different diffusion pathways as follows:

$$\varepsilon_k = \frac{ar_s + br_b}{r_s + r_b + r_a},\ ‰ \tag{20}$$

where r_s, r_b and r_a are stomatal, boundary layer and aerodynamic resistance. The coefficients *a* and *b* refer to the molecular kinetic factor (32‰ for $^1H_2{}^{18}O$ and 16‰ for $^1H^2H^{16}O$) and the kinetic factor associated with the leaf boundary layer (21‰ for $^1H_2{}^{18}O$ and 11‰ for $^1H^2H^{16}O$) (Cappa et al., 2003; Farquhar et al., 1989). Readers are reminded that the coefficients change if the experimental results of Merlivat (1978) are employed. The results of in situ observations and modeling research show that air turbulence is indeed a contributing factor (Xiao et al., 2010, 2012).

5.5. Water mass balance method

If the isotopic composition of leaf water is sampled at short time intervals, δ_T can be calculated from the leaf water mass balance (Hu et al., 2014). Because the variation in leaf water content depends only on water entering and exiting the leaves, the transpiration rate can be calculated as follows:

$$T = X - \frac{\Delta L_w}{dt} \tag{21}$$

where *X* represents the water flux through the stem, L_w is the leaf water content, and the second right-hand item in the equation represents the temporal rate of variation in leaf water content. Leaf water content was usually calculated as the mass difference between fresh leaves and dry leaves with reference to the leaf area.

The isotopic mass balance can be written as follows:

$$\delta_T T = \delta_X X - \Delta(\delta_{L,b} L_w) \tag{22}$$

where δ_T, δ_X and $\delta_{L,b}$ represent the isotopic composition of plant transpiration, stem xylem water and leaf water, respectively.

Combining Eqs. (21) and (22), δ_T can be solved as follows:

$$\delta_T = \frac{[\delta_X(T + \Delta L_w) - \Delta(\delta_{L,b} L_w)]}{T} \tag{23}$$

To use this method, the sampling interval should be short to ensure that δ_T and δ_X do not change during the interval. This method was used to estimate the δ_T of a temperate grassland and an oasis maize cropland (Hu et al., 2014; Wen et al., 2016).

5.6. Uncertainty in δ_T estimation

Comparison of the wheat canopy $\delta^{18}O_T$ at the Luancheng site in China simulated using the non-steady-state model and under the steady-state assumption is shown in Fig. 6. The scattered hourly data points (gray dots) indicate a clear deviation from the steady-state. The canopy is close to steady-state only at midday (11:00–13:00 local time), with a small deviation of -0.7 ± 1.5‰. In the morning (8:00–10:00) and afternoon (13:00–17:00), the δ_T is higher than the δ_X, with a mean bias of 2.0 ± 8.0‰ and 1.1 ± 4.6‰, respectively.

The comparison of the δ_T calculated using non-steady-state models and under the steady-state assumptions over crops, grassland and forests in the previous literature are shown in Fig. 7. The results indicated that δ_T reaches the steady-state from late morning to afternoon and is

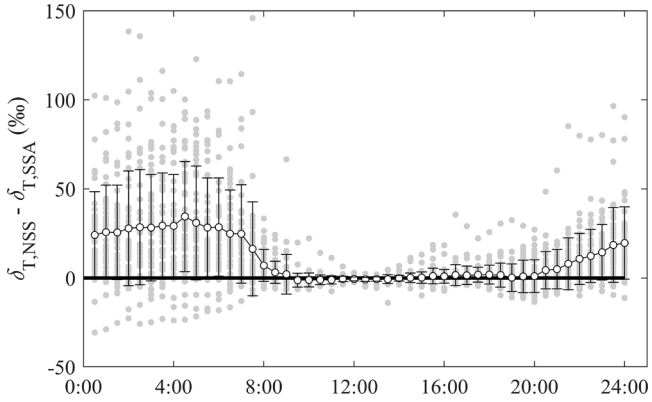

Fig. 6. Comparison of $\delta^{18}O_T$ values simulated using the model under non-steady-state (Farquhar and Cernusak, 2005) ($\delta_{T,NSS}$) and steady-state assumptions ($\delta_{T,SSA}$) based on the data of a wheat canopy at the Luancheng site in China (Xiao et al., 2012) (gray dots, original data; circles: mean value; error bars: 1 standard deviation).

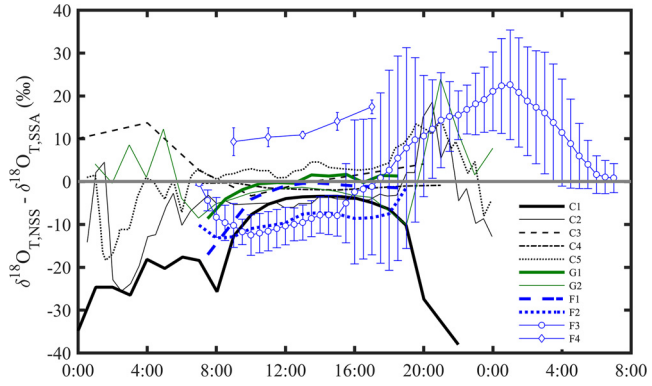

Fig. 7. Comparison of $\delta^{18}O_T$ values simulated using the model under non-steady-state ($\delta_{T,NSS}$) and steady-state assumptions ($\delta_{T,SSA}$) over crops [C1–C5: Wang et al. (2016); Welp et al. (2008); Wen et al. (2016); Wu et al. (2017); Xiao et al. (2010)], grassland [G1–G2: Hu et al. (2014); Wang et al. (2015)] and forests [F1–F4: Dubbert et al. (2013); Lai et al. (2006); Dubbert et al. (2014a); Sun et al. (2014)].

not in a steady-state at other times. For example, the study by Dubbert et al. (2013) indicates that δ_T of a savanna-oak woodland is not in a steady-state during the morning but reaches the steady-state in the afternoon (14:00–18:00). A modeling study of a grassland ecosystem by Wang et al. (2015) indicates that δ_T is close to steady-state during midday. The observation by Welp et al. (2008) indicates that δ_{ET} was close to steady-state to within approximately 3‰, between 10:00 and 16:00 in a soybean system.

6. Uncertainties in *ET* partitioning via the isotopic method

The uncertainty of f_T estimations using the two-source mixing model is directly related to the uncertainty in all three of the terms: δ_{ET}, δ_T, and δ_E (Good et al., 2014; Wei et al., 2015). The effects of uncertainties of δ_{ET}, δ_T, and δ_E mentioned above on *T/ET* partitioning at different growth stages are usually quantified by a first-order Taylor series expansion of the final partitioned value uncertainties (Good et al., 2014; Phillips and Gregg, 2001; Wei et al., 2015):

$$\sigma_{f_T}^2 = \frac{\sigma_{\delta_{ET}}^2}{(\delta_T - \delta_E)^2} + f_T \frac{\sigma_{\delta_T}^2}{(\delta_T - \delta_E)^2} + (1 - f_T)\frac{\sigma_{\delta_E}^2}{(\delta_T - \delta_E)^2} \quad (24)$$

where $\sigma_{\delta_{ET}}^2$, $\sigma_{\delta_T}^2$ and $\sigma_{\delta_E}^2$ represent variances in the mean isotopic compositions of *ET*, *T* and *E*, respectively. Using the maize field data reported by Wei et al. (2018) and assuming that the values of $\sigma_{\delta_{ET}}$, σ_{δ_T} and σ_{δ_E} are the standard deviations for each day (10:00–16:00 local time), Fig. 8 depicts the fractional contribution to the total variance of the uncertainties of f_T (σ_{f_T}). Generally, σ_{δ_T} is small because only midday data were selected. Therefore, the uncertainty of δ_T is less important than that of δ_{ET} and δ_E. Under low f_T conditions, partitioning uncertainty is caused mostly by the uncertainty of δ_{ET}, as δ_{ET} is more poorly quantified under low evapotranspiration conditions. As f_T increases, uncertainties in δ_E and δ_{ET} both reduce the accuracy of f_T. This finding implies that further improvement in δ_E and δ_{ET} estimations is required for partitioning evapotranspiration using the isotopic method. The uncertainties shown in Fig. 8 are likely upper bounds of measurement errors because some of the calculated $\sigma_{\delta_{ET}}$, σ_{δ_T} and σ_{δ_E} are caused by natural variations in these endmembers at the sub-day time scale.

Fig. 8 applies to the maize field conditions described by Wei et al. (2018). To obtain a broader sense of error propagation, we consider two synthetic datasets in this study. The first one is a forest scenario with end members as $\delta_{ET} = -9$‰, $\delta_T = -5$‰, $\delta_E = -25$‰, giving a transpiration ratio of $T/ET = 80\%$. The second scenario is a crop scenario ($T/ET = 50\%$, $\delta_{ET} = -15$‰, $\delta_T = -5$‰, $\delta_E = -25$‰). Next, we survey the published literature on the uncertainties of the three end members, obtaining mean uncertainties of 5.1‰, 2.7‰, and 0.8‰ for δ_{ET}, δ_E, and δ_T, respectively (Table A2). The relative contributions to the overall uncertainty in *T/ET* from these scenarios (open symbols, Fig. 8) are consistent with the results shown for the maize field. In addition, we performed a Monte Carlo error propagation analysis using a total of 800,000 ensemble members and assuming a normal distribution of errors. The overall uncertainty for *T/ET* is ± 21% (one standard deviation) for both scenarios.

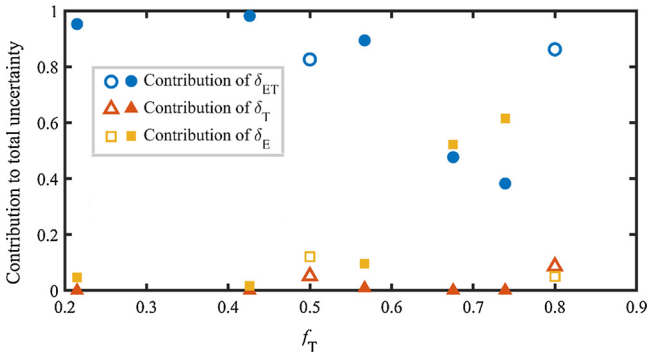

Fig. 8. Contribution of uncertainty in δ_{ET}, δ_E and δ_T to the total uncertainty of the *ET* partitioning. Solid symbols denote the conditions in the maize field described by Wei et al. (2018), and open symbols denote synthetic experiments with typical uncertainties found in the literature.

The fractional contribution to the total variance in uncertainties of f_T can vary under different field conditions. For example, Wei et al. (2015) reported that during the early growing season, σ_{δ_T} is quite large, whereas δ_{ET} plays a dominant role after the late growing season. Good et al. (2014) reported that partitioning uncertainty at low values of f_T is due mostly to uncertainty in δ_{ET}, while both uncertainties in δ_T and δ_{ET} have a great impact as f_T increases. The uncertainty analysis presented here is also a statistical analysis based on the assumption that the source and final values are independently measured. The uncertainty associated with different parameterizations (kinetic fractionation factors) and assumptions [non-steady-state (NSS) or steady-state assumption (SS) in δ_T estimation as well as Keeling plot or gradient approaches in δ_{ET} estimation] should also be considered.

Finally, a complication exists if the plant foliar takes up atmospheric moisture under conditions of near saturation, such as during fog events (Limm et al., 2009; Goldsmith et al., 2017). When this occurs, the two-source mass balance framework does not hold strictly because atmospheric moisture is now a third end member.

7. Discrepancies in different *ET* partitioning approaches

Discrepancies in the ecosystem *T/ET* estimation using different *ET* partitioning approaches have been reported by Berkelhammer et al. (2016); Kool et al. (2014); Schlesinger and Jasechko (2014); Sutanto et al. (2014) and Wei et al. (2018). In general, the discrepancies can be mainly explained by multiple sources of uncertainties related to measurement errors, validity of assumptions, different footprints and field heterogeneity (Wei et al., 2018). For example, WUE-based partitioning avoids the problem of scale mismatch. However, the determination of potential WUE, which is a key parameter in this approach, requires periods with $T/ET = 1$ (Zhou et al., 2016) or multiyear measurement data on carbon and water fluxes (Scott and Biederman, 2017) as a reference. It is also known that even though transpiration or evaporation at a small scale (such as the leaf scale) can be accurately determined based on measurements of sap-flow, leaf conductance and soil chamber, large errors may occur when these measurements are upscaled to the ecosystem level.

As mentioned in the previous section, the isotopic method also faces several challenges. The development of laser spectroscopy technology makes it possible for continuous measurements of the isotopic compositions of both water vapor and soil/plant water at high temporal resolutions (Oerter et al., 2017; Rothfuss et al., 2015; Volkmann et al., 2016). By increasing the temporal repetitions, this technique may provide us with the opportunity to improve the estimation of δ_E and the accuracy of *ET* partitioning. Improved parameterizations of the fractionation mechanisms involved in soil evaporation and plant transpiration can also emerge from coordinated field observations, where the isotopic method is deployed simultaneously with other traditional methods.

8. Conclusions

The stable isotope method is a powerful tool for evapotranspiration partitioning. This review focuses on the isotopic method of *ET* partitioning based on the framework of a two-source model, with the isotope compositions of *E*, *T* and *ET* being the key measurement variables. Previous reports of isotope-based *ET* partitioning showed various *T/ET* values among different ecosystems. Accurate estimation of δ_{ET}, δ_E and δ_T is vital for *ET* partitioning. Regarding the estimation of δ_{ET}, each method (chamber, eddy covariance, Keeling plot and gradient-flux method) has its own limitations and assumptions, which should be fully

considered before selection. For the estimation of δ_E, the parameterization of the soil fractionation factor and estimation of the isotopic composition of evaporation sites in the soil are key issues. The estimation of δ_T should consider the following issues: steady-state versus non-steady-state assumption, well-mixed assumption versus the Péclet effect, and the role of turbulence on the canopy kinetic fractionation effect. Coordinated field observations, where the isotopic method is deployed simultaneously with other traditional methods, are needed to improve parameterizations of the fractionation mechanisms involved in soil evaporation and plant transpiration.

Acknowledgments

This work was supported by the National Key R&D Program of China (grant number 2017YFC0503904), the National Natural Science Foundation of China (grant number 41475141, 41505005), the U.S. National Science Foundation (grant number 1520684), the Ministry of Education of China (grant number PCSIRT), and the Priority Academic Program Development of Jiangsu Higher Education Institutions (grant number PAPD). We would also like to thank the reviewers, especially one anonymous reviewer for their valuable and constructive comments and suggestions, which helped improve the quality of this manuscript significantly.

Appendix A

Table A1

Table A1
Notations.

Notation	Meaning
C_{bg}	The background atmospheric water vapor concentration (kg m^{-3})
C_{ET}	The water vapor contributed by the ecosystem evapotranspiration (kg m^{-3})
C_M	The water vapor concentration of the air inside the chamber (kg m^{-3})
C_V	The water vapor concentration of the ambient atmosphere (kg m^{-3})
D_v	The molecular diffusivity of $^1H_2{}^{16}O$ (m^2 s^{-1})
D_v^i	The molecular diffusivity of $^1H_2{}^{18}O$ or $^1H^2H^{16}O$ (m^2 s^{-1})
E	Evaporation (mol m^{-2} s^{-1})
ET	Evapotranspiration (mol m^{-2} s^{-1})
F_{ET}	The water vapor flux of $^1H_2{}^{16}O$ (mol m^{-2} s^{-1})
F'_{ET}	The water vapor flux of $^1H_2{}^{18}O$ or $^1H^2H^{16}O$ (mol m^{-2} s^{-1})
F_x	The molar flux of $^1H_2{}^{16}O$ (mol m^{-2} s^{-1})
F_x'	The molar flux of the minor isotopic water molecules ($^1H^2HO$ or $^1H_2{}^{18}O$) (mol m^{-2} s^{-1})
f_T	The ratio of T to ET (dimensionless)
h	The atmospheric relative humidity in reference to the water surface temperature (dimensionless)
K	Eddy diffusivity (m^2 s^{-1})
LAI	Leaf area index (dimensionless)
L_w	The leaf water content (mol m^{-2})
M_V	The molar mass of $^1H_2{}^{16}O$ (kg mol^{-1})
M'_V	The molar mass of $^1H_2{}^{18}O$ (or $^1H^2H^{16}O$) (kg mol^{-1})
n	Exponent of diffusivity (dimensionless)
n_a	Atmosphere-controlled exponent of diffusivity, = 0.67 (dimensionless)
n_s	Soil-controlled exponent of diffusivity, = 1 (dimensionless)
R_E	The (either oxygen or hydrogen) stable isotopic ratios of soil evaporation (dimensionless)
R_{ET}	The (either oxygen or hydrogen) stable isotopic ratios of ecosystem evapotranspiration (dimensionless)
R_T	The (either oxygen or hydrogen) stable isotopic ratios of transpiration (dimensionless)
R_{VSMOW}	The $^2H/^1H$ or $^{18}O/^{16}O$ molar ratio of the Vienna Standard Mean Ocean Water, whose values are 0.00015576 and 0.0020052, respectively (dimensionless)
R_x	The water vapor flux hydrogen or oxygen stable isotopic ratio (dimensionless)
r_a	Aerodynamic resistance
r_b	Boundary layer resistance (m^2s mol^{-1})
r_s	Stomatal resistance (m^2s mol^{-1})
T	Transpiration (mol m^{-2} s^{-1})
t	Time (s)
w	Vertical wind velocity (m s^{-1})
X	The water flux through the stem (mol m^{-2} s^{-1})
α_{eq}	The equilibrium fractionation factor (> 1) (dimensionless)
δ_{bg}	The isotopic composition of background atmospheric water vapor concentration (‰)
δ_E	The (either oxygen or hydrogen) stable isotopic compositions of soil evaporation (‰)
δ_{ET}	The (either oxygen or hydrogen) stable isotopic compositions of ecosystem evapotranspiration (‰)
δ_F	The isotopic composition of water vapor flux (‰)

(*continued on next page*)

Table A1 (*continued*)

Notation	Meaning
δ_L	The isotopic composition of evaporation front (‰)
$\delta_{L,b}$	The isotopic composition of leaf water (‰)
δ_M	The isotopic composition of water vapor inside the chamber (‰)
δ_s	The isotopic composition of soil water (‰)
δ_T	The (either oxygen or hydrogen) stable isotopic compositions of plant transpiration (‰)
δ_V	The isotopic composition of atmospheric water vapor or outside the chamber (‰)
δ_X	The isotopic composition of stem xylem water (‰)
ΔC	The difference in the water vapor concentration at the two heights (kg m^{-3})
$\Delta C'$	The $^1H_2{}^{18}O$ (or $^1H^2H^{16}O$) molar difference at the two heights (kg m^{-3})
Δz	Height difference (m)
ε_{eq}	The equilibrium fractionation, equal to $(1–1/\alpha_{eq}) \times 10^3$ (‰)
ε_k	The kinetic fractionation (‰)
θ_r	Residual volumetric water content (dimensionless)
θ_{sat}	Saturation volumetric water content (dimensionless)
θ_{surf}	Volumetric water content at the surface (dimensionless)
$\sigma_{\delta E}$	Standard deviation of the mean isotopic compositions for evaporation
$\sigma_{\delta ET}$	Standard deviation of the mean isotopic compositions for evapotranspiration
$\sigma_{\delta T}$	Standard deviation of the mean isotopic compositions for transpiration
σ_{fT}	Uncertainty of f_T
$\hat{\chi}_{a,1}$	The true values of the molar mixing ratio of $^1H_2{}^{16}O$ at height 1 (mol mol^{-1})
$\hat{\chi}'_{a,1}$	The true values of the molar mixing ratio of $^1H_2{}^{18}O$ (or $^1H^2H^{16}O$) at height 1 (mol mol^{-1})
$\hat{\chi}_{a,2}$	The true values of the molar mixing ratio of $^1H_2{}^{16}O$ at height 2 (mol mol^{-1})
$\hat{\chi}'_{a,2}$	The true values of the molar mixing ratio of $^1H_2{}^{18}O$ (or $^1H^2H^{16}O$) at height 2 (mol mol^{-1})
χ_{bg}	The molar mixing ratio of water vapor of the background atmosphere (mol mol^{-1})
χ_v	The molar mixing ratio of water vapor (mol of water molecules in 1 mol of dry air) (mol mol^{-1})
$\overline{w'\chi'_V}$	The covariance of the vertical wind velocity w and χ_v (m s^{-1}·mol mol^{-1})
$\overline{w'\delta'_V}$	The isoforcing (‰ m s^{-1})

Table A2
Literature survey on the uncertainties of the δ_{ET}, δ_T and δ_E estimation in the literature.

δ_{ET}		δ_E		δ_T	
Uncertainty (‰)	References	Uncertainty (‰)	Reference	Uncertainty (‰)	Reference
1.4	(Lee et al., 2007)	0.15**	(Rothfuss et al., 2010)	0.15–0.30**	(Rothfuss et al., 2010)
5.83	(Good et al., 2012)	2.2*	(Good et al., 2014)	0.1–0.5	(Wei et al., 2018)
5.89	(Good et al., 2012)	< 5	(Hu et al., 2014)	< 1	(Hu et al., 2014)
3.1*	(Good et al., 2014)	1–5	(Dubbert et al., 2013)		
4.6 (0.2–35.2)	(Huang and Wen, 2014; Wen et al., 2016)			1.6 (0.8–3.3)	(Welp et al., 2008)
7.9 (0.8–53)	(Hu et al., 2014)			5.9*	(Good et al., 2014)
< 19.4*	(Wang et al., 2015)			0.7	(Dubbert et al., 2013)
5.1	Average	2.7	Average	0.8	Average

* Ignored in the average calculation.
** Climatic chamber.

References

Allison, G.B., Barnes, C.J., 1983. Estimation of evaporation from non-vegetated surfaces using natural deuterium. Nature 301, 143–145.

Aouade, G., Ezzahar, J., Amenzou, N., Er-Raki, S., Benkaddour, A., Khabba, S., Jarlan, L., 2016. Combining stable isotopes, Eddy Covariance system and meteorological measurements for partitioning evapotranspiration, of winter wheat, into soil evaporation and plant transpiration in a semi-arid region. Agric. Water Manage. 177, 181–192. https://doi.org/10.1016/j.agwat.2016.07.021.

Baldocchi, D.D., Hicks, B.B., Meyers, T.P., 1988. Measuring biosphere-atmosphere exchanges of biologically related gases with micrometeorological methods. Ecology 69, 1331–1340.

Barnes, C.J., Allison, G.B., 1983. The distribution of deuterium and ^{18}O in dry soils. J. Hdrol. 60, 141–156.

Barnes, C.J., Allison, G.B., 1988. Tracing of water movement in the unsaturated zone using stable isotopes of hydrogen and oxygen. J. Hydrol. (Amst.) 100, 143–176.

Berkelhammer, M., Noone, D.C., Wong, T.E., Burns, S.P., Knowles, J.F., Kaushik, A., Blanken, P.D., Williams, M.W., 2016. Convergent approaches to determine an ecosystem's transpiration fraction. Global Biogeochem. Cycles 30, 933–951. https://doi.org/10.1002/2016GB005392.

Braud, I., Bariac, T., Gaudet, J.P., Vauclin, M., 2005. SiSPAT-Isotope, a coupled heat, water and stable isotope (HDO and $H_2{}^{18}O$) transport model for bare soil. Part I. Model description and first verifications. J. Hydrol. (Amst.) 309, 277–300. https://doi.org/10.1016/j.jhydrol.2004.12.013.

Braud, I., Bariac, T., Biron, P., Vauclin, M., 2009a. Isotopic composition of bare soil

evaporated water vapor. Part II: modeling of RUBIC IV experimental results. J. Hydrol. (Amst.) 369, 17–29. https://doi.org/10.1016/j.jhydrol.2009.01.038.
Braud, I., Biron, P., Bariac, T., Richard, P., Canale, L., Gaudet, J.P., Vauclin, M., 2009b. Isotopic composition of bare soil evaporated water vapor. Part I: RUBIC IV experimental setup and results. J. Hydrol. (Amst.) 369, 1–16. https://doi.org/10.1016/j.jhydrol.2009.01.034.
Brunel, J.P., Walker, G.R., Dighton, J.C., Monteny, B., 1997. Use of stable isotopes of water to determine the origin of water used by the vegetation and to partition evapotranspiration. A case study from HAPEX-Sahel. J. Hydrol. (Amst.) 188–189, 466–481.
Cappa, C.D., Hendrichs, M.B., DePaolo, D.J., Cohen, R.C., 2003. Isotopic fractionation of water during evaporation. J. Geophys. Res. 108, 4525. https://doi.org/10.1029/2003JD003597.
Cernusak, L.A., Farquhar, G.D., Pate, J.S., 2005. Environmental and physiological controls over oxygen and carbon isotope composition of Tasmanian blue gum, Eucalyptus globulus. Tree Physiol. 25, 129–146.
Chen, Y., Xia, J., Liang, S., Feng, J., Fisher, J.B., Li, X., Li, X., Liu, S., Ma, Z., Miyata, A., et al., 2014. Comparison of satellite-based evapotranspiration models over terrestrial ecosystems in China. Remote Sens. Environ. 140, 279–293.
Coenders-Gerrits, A.M.J., van der Ent, R.J., Bogaard, T.A., Wang-Erlandsson, L., Hrachowitz, M., Savenije, H.H.G., 2014. Uncertainties in transpiration estimates. Nature 496, 347–350.
Coplen, T.B., 2011. Guidelines and recommended terms for expression of stable-isotope-ratio and gas-ratio measurement results. Rapid Commun. Mass Spectrom. 25, 2538–2560. https://doi.org/10.1002/Rcm.5129.
Craig, H., Gordon, L.I., 1965. Deuterium and oxygen-18 variations in the ocean and the marine atmosphere. Tongiorgi, E. (Ed.), Proceedings of the Conference on Stable Isotopes in Oceanographic Studies and Paleotemperatures. 9–130.
Cuntz, M., Ciais, P., Hoffmann, G., Knorr, W., 2003. A comprehensive global three-dimensional model of $\delta^{18}O$ in atmospheric CO_2: 1. Validation of surface processes. J. Geophys. Res. 108, 4527. https://doi.org/10.1029/2002JD003153.
Dongmann, G., Nurnberg, H.W., Forstel, H., Wagener, K., 1974. On the enrichment of $H_2{}^{18}O$ in the leaves of transpiring plants. Radiat. Environ. Biophys. 11, 41–52. https://doi.org/10.1007/BF01323099.
Dubbert, M., Cuntz, M., Piayda, A., Maguás, C., Werner, C., 2013. Partitioning evapotranspiration – testing the Craig and Gordon model with field measurements of oxygen isotope ratios of evaporative fluxes. J. Hydrol. (Amst) 496, 142–153. https://doi.org/10.1016/j.jhydrol.2013.05.033.
Dubbert, M., Cuntz, M., Piayda, A., Werner, C., 2014a. Oxygen isotope signatures of transpired water vapor: the role of isotopic non-steady-state transpiration under natural conditions. New Phytol. 203, 1242–1252. https://doi.org/10.1111/nph.12878.
Dubbert, M., Piayda, A., Cuntz, M., Correia, A.C., e Silva, F.C., Pereira, J.S., Werner, C., 2014b. Stable oxygen isotope and flux partitioning demonstrates understory of an oak savanna contributes up to half of ecosystem carbon and water exchange. Front. Plant Sci. 5, 530. https://doi.org/10.3389/fpls.2014.00530.
Dubbert, M., Kübert, A., Werner, C., 2017. Impact of leaf traits on temporal dynamics of transpired oxygen isotope signatures and its impact on atmospheric vapor. Front. Plant Sci. 8, 5. https://doi.org/10.3389/fpls.2017.00005.
Ellsworth, P.Z., Williams, D.G., 2007. Hydrogen isotope fractionation during water uptake by wood xerophytes. Plant Soil 291, 93–107. https://doi.org/10.1007/s11104-006-9177-1.
Farquhar, G.D., Cernusak, L.A., 2005. On the isotopic composition of leaf water in the non-steady state. Funct. Plant Biol. 32, 293–303. https://doi.org/10.1071/Fp04232.
Farquhar, G.D., Lloyd, J., 1993. Carbon and oxygen isotope effects on the exchange of carbon dioxide between plants and the atmosphere. In: Ehleringer, J.R., Hall, A.E., Farquhar, G.D. (Eds.), Stable Isotopes and Plant Carbon/Water Relations. Academic, San Diego, pp. 47–70.
Farquhar, G.D., Hubick, K.T., Condon, A.G., Richards, R.A., 1989. Carbon isotope discrimination and water-use efficiency. In: Rundel, P.W., Ehleringer, J.R., Nagy, K.A. (Eds.), Stable Isotopes in Ecological Research. Springer-Verlag, New York, pp. 21–46.
Farquhar, G.D., Cernusak, L.A., Barnes, B., 2007. Heavy water fractionation during transpiration. Plant Physiol. 143, 11–18.
Farris, F., Strain, B.R., 1978. The effects of water stress on leaf $H_2{}^{18}O$ enrichment. Radiat. Environ. Biophys. 15, 167–202.
Ferretti, D.F., Pendall, E., Morgan, J.A., Nelson, J.A., LeCain, D., Mosier, A.R., 2003. Partitioning evapotranspiration fluxes from a Colorado grassland using stable isotopes: seasonal variations and ecosystem implications of elevated atmospheric CO_2. Plant Soil 254, 291–303.
Flanagan, L.B., Comstock, J.P., Ehleringer, J.R., 1991. Comparison of modeled and observed environmental influences on the stable oxygen and hydrogen isotope composition of leaf water in *Phaseolus vulgaris* L. Plant Physiol. 96, 588–596.
Flanagan, L.B., Marshall, J.D., Ehleringer, J.R., 1993. Photosynthetic gas exchange and the stable isotope composition of leaf water: comparison of a xylem-tapping mistletoe and its host. Plant Cell Environ. 16, 623–631.
Forstel, H., 1978. The enrichment of ^{18}O in leaf water under natural conditions. Radiat. Environ. Biophys. 15, 323–344.
Gat, J.R., Bowser, C.J., et al., 1991. Heavy isotope enrichment in coupled evaporative systems. In: In: Taylor, H.P. (Ed.), Stable Isotope Geochemistry: A Tribute to Samuel Epstein, vol. 3. Spec. Publ. Geochem. Soc., pp. 159–168.
Gibson, J.J., Edwards, T.W.D., 2002. Regional water balance trends and evaporation-transpiration partitioning from a stable isotope survey of lakes in northern Canada. Global Biogeochem. Cycles 16, 1026. https://doi.org/10.1029/2001GB001839.
Goldsmith, G.R., Lehmann, M.M., Cernusak, L.A., Arend, M., Siegwolf, R.T.W., 2017. Inferring foliar water uptake using stable isotopes of water. Oecologia 184, 763–766. https://doi.org/10.1007/s00442-017-3917-1.
Good, S.P., Soderberg, K., Wang, L., Caylor, K.K., 2012. Uncertainties in the assessment of the isotopic composition of surface fluxes: a direct comparison of techniques using laser-based water vapor isotope analyzers. J. Geophys. Res. 117, D15301. https://doi.org/10.1029/2011JD017168.
Good, S.P., Soderberg, K., Guan, K., King, E.G., Scanlon, T.M., Caylor, K.K., 2014. δ^2H isotopic flux partitioning of evapotranspiration over a grass field following a water pulse and subsequent dry down. Water Resour. Res. 50, 1410–1432. https://doi.org/10.1002/2013wr014333.
Good, S.P., Noone, D., Bowen, G., 2015. Hydrologic connectivity constrains partitioning of global terrestrial water fluxes. Science 349, 175–177. https://doi.org/10.1126/science.aaa5931.
Good, S.P., Moore, G.W., Miralles, D.G., 2017. A mesic maximum in biological water use demarcates biome sensitivity to aridity shifts. Nat. Ecol. Evol. 1, 1883–1888. https://doi.org/10.1038/s41559-017-0371-8.
Griffis, T.J., 2013. Tracing the flow of carbon dioxide and water vapor between the biosphere and atmosphere: a review of optical isotope techniques and their application. Agric. For. Meteorol. 174–175, 85–109. https://doi.org/10.1016/j.agrformet.2013.02.009.
Griffis, T.J., Baker, J.M., Sargent, S.D., Tanner, B.D., Zhang, J., 2004. Measuring field-scale isotopic CO_2 fluxes with tunable diode laser absorption spectroscopy and micrometeorological techniques. Agric. For. Meteorol. 124, 15–29. https://doi.org/10.1016/j.agrformet.2004.01.009.
Griffis, T.J., Lee, X., Baker, J.M., Sargent, S.D., King, J.Y., 2005. Feasibility of quantifying ecosystem-atmosphere $C^{18}O^{16}O$ exchange using laser spectroscopy and the flux-gradient method. Agric. For. Meteorol. 135, 44–60. https://doi.org/10.1016/j.agrformet.2005.10.002.
Griffis, T.J., Zhang, J., Baker, J.M., Kljun, N., Billmark, K., 2007. Determining carbon isotope signatures from micrometeorological measurements: implications for studying biosphere-atmosphere exchange process. Boundary-Layer Meteorol. 123, 295–316. https://doi.org/10.1007/s10546-006-9143-8.
Griffis, T.J., Sargent, S.D., Baker, J.M., Lee, X., Tanner, B.D., Greene, J., Swiatek, E., Billmark, K., 2008. Direct measurement of biosphere-atmosphere isotopic CO_2 exchange using the eddy covariance technique. J. Geophys. Res. 113, D08304. https://doi.org/10.1029/2007JD009297.
Griffis, T.J., Sargent, S.D., Lee, X., Baker, J.M., Greene, J., Erickson, M., Zhang, X., Billmark, K., Schultz, N., Xiao, W., Hu, N., 2010. Determining the oxygen isotope composition of evapotranspiration using eddy covariance. Boundary Layer Meterol. 137 (2), 307–326. https://doi.org/10.1007/s10546-010-9529-5.
Hoffmann, G., Cuntz, M., Weber, C., Ciais, P., Friedlingstein, P., Heimann, M., Jouzel, J., Kaduk, J., Maier-Reimer, E., Seibt, U., Six, K., 2004. A model of the Earth's Dole effect. Global Biogeochem. Cycles 18, GB1008 https://doi.org/1029/2003GB002059.
Hsieh, J.C.C., Chadwick, O.A., Kelly, E.F., Savin, S.M., 1998. Oxygen isotopic composition of soil water: quantifying evaporation and transpiration. Geoderma 82, 269–293.
Hu, Z., Wen, X., Sun, X., Li, L., Yu, G., Lee, X., Li, S., 2014. Partitioning of evapotranspiration through oxygen isotopic measurements of water pools and fluxes in a temperate grassland. J. Geophys. Res. Biogeosci. 119, 358–371. https://doi.org/10.1002/2013jg002367.
Huang, L., Wen, X., 2014. Temporal variations of atmospheric water vapor δD and $\delta^{18}O$ above an arid artificial oasis cropland in the Heihe River Basin. J. Geophys. Res. Atmos. 119, 11456–11476. https://doi.org/10.1002/2014JD021891.
Jasechko, S., Sharp, Z.D., Gibson, J.J., Birks, S.J., Yi, Y., Fawcett, P.J., 2013. Terrestrial water fluxes dominated by transpiration. Nature 496, 347–350. https://doi.org/10.1038/nature11983.
Jefferson, J.L., Maxwell, R.M., Constantine, P.G., 2017. Exploring the sensitivity of photosynthesis and stomatal resistance parameters in a Land Surface Model. J. Hydrometeorol. 18, 897–915. https://doi.org/10.1175/JHM-D-16-0053.1.
Keeling, C.D., 1958. The concentration and isotopic abundances of carbon dioxide in rural areas. Geochim. Cosmochim. Acta 13, 322–334.
Kelliher, F.M., Köstner, B.M.M., Hollinger, D.Y., Byers, J.N., Hunt, J.E., McSeveny, T.M., Meserth, R., Weir, P.L., Schulze, E.D., 1992. Evaporation, xylem sap flow, and tree transpiration in a New Zealand broad-leaved forest. Agric. For. Meteorol. 62, 53–73.
Kochendorfer, J.P., Ramírez, J.A., 2010. Ecohydrologic controls on vegetation density and evapotranspiration partitioning across the climatic gradients of the central United States. Hydrol. Earth Syst. Sci. Discuss. 14, 2121–2139.
Kool, D., Agam, N., Lazarovitch, N., Heitman, J.L., Sauer, T.J., Ben-Gal, A., 2014. A review of approaches for evapotranspiration partitioning. Agric. For. Meterol. 184, 56–70.
Lai, C.T., Ehleringer, J.R., Bond, B.J., Paw U, K.T., 2006. Contributions of evaporation, isotopic non-steady state transpiration and atmospheric mixing on the $\delta^{18}O$ of water vapour in Pacific Northwest coniferous forests. Plant Cell Environ. 29, 77–94. https://doi.org/10.1111/j.1365-3040.2005.01402.x.
Leaney, F.W., Osmond, C.B., Allison, G.B., Ziegler, H., 1985. Hydrogen-isotope composition of leaf water in C_3 and C_4 plants: its relationship to the hydrogen-isotope composition of dry matter. Planta 164, 215–220.
Lee, X., 2018. Fundamentals of Boundary-Layer Meteorology. Springer, Berlin.
Lee, X., Smith, R., Williams, J., 2006. Water vapour $^{18}O/^{16}O$ isotope ratio in surface air in New England. USA. Tellus 58B, 293–304. https://doi.org/10.1111/j.1600-0889.2006.00191.x.
Lee, X., Kim, K., Smith, R., 2007. Temporal variations of the $^{18}O/^{16}O$ signal of the whole-canopy transpiration in a temperate forest. Global Biogeochem. Cycles 21, GB3013. https://doi.org/10.1029/2006GB002871.
Lee, X., Griffis, T.J., Baker, J.M., Billmark, K.A., Kim, K., Welp, L., 2009. Canopy-scale kinetic fractionation of atmospheric carbon dioxide and water vapor isotopes. Global Biogeochem. Cycles 23, GB1002. https://doi.org/10.1029/2008GB003331.
Lee, D., Kim, J., Lee, K.S., Kim, S., 2010. Partitioning of catchment water budget and its

implications for ecosystem carbon exchange. Biogeosciences 7, 1903–1914. https://doi.org/10.5194/bg-7-1903-2010.
Lee, X., Huang, J., Patton, E.G., 2012. A large-eddy simulation study of water vapour and carbon dioxide isotopes in the atmospheric boundary layer. Bound.-Layer Meteorol. 145, 229–248. https://doi.org/10.1007/s10546-011-9631-3.
Limm, E.B., Simonin, K.A., Bothman, A.G., Dawson, T.E., 2009. Foliar water uptake: a common water acquisition strategy for plants of the redwood forest. Oecologia 161 (3), 449–459. https://doi.org/10.1007/s00442-009-1400-3.
Lu, X., Liang, L.L., Wang, L., Jenerette, G.D., McCabe, M.F., Grantz, D.A., 2017. Partitioning of evapotranspiration using a stable isotope technique in an arid and high temperature agricultural production system. Agric. Water Manage. 179, 103–109. https://doi.org/10.1016/j.agwat.2016.08.012.
Luz, B., Barkan, E., Yam, R., Shemesh, A., 2009. Fractionation of oxygen and hydrogen isotopes in evaporating water. Geochim. Cosmochim. Acta 73, 6697–6703. https://doi.org/10.1016/j.gca.2009.08.008.
Majoube, M., 1971. Fractionnement en oxygene-18 et en deuterium entre l'eau et sa vapeur. J. Chim. Phys. Physicochim. Biol. 68, 1423–1436.
Martens, B., Miralles, D.G., Lievens, H., van der Schalie, R., De Jeu, R.A.M., Fernández-Prieto, D., Beck, H.E., Dorigo, W.A., Verhoest, N.E., 2017. GLEAM v3: satellite-based land evaporation and root-zone soil moisture. Geosci. Model. Dev. Discuss. 10, 1903–1925. https://doi.org/10.5194/gmd-10-1903-2017.
Mathieu, R., Bariac, T., 1996. A numerical model for the simulation of stable isotope profiles in drying soils. J. Geophys. Res. 101, 12685–12696.
Merlivat, L., 1978. Molecular diffusivities of $H_2{}^{16}O$, $HDO^{16}O$, and $H_2{}^{18}O$ in gases. J. Chem. Phys. 69, 2864–2871.
Merlivat, L., Botter, R., Nief, G., 1963. Fractionnement isotopique au cours de la distillation de l'eau. J. Chim. Phys. Physicochim. Biol. 60, 56.
Miralles, D.G., De Jeu, R.A.M., Gash, J.H., Holmes, T.R.H., Dolman, A.J., 2011. Magnitude and variability of land evaporation and its components at the global scale. Hydrol. Earth Syst. Sci. Discuss. 15, 967–981. https://doi.org/10.5194/hess-15-967-2011.
Moreira, M.Z., Sternberg, L.D.S.L., Martinelli, L.A., Victoria, R.L., Barbosa, E.M., Bonates, L.C.M., Nepstad, D.C., 1997. Contribution of transpiration to forest ambient vapour based on isotopic measurements. Glob. Change Biol. Bioenergy 3, 439–450.
Oerter, E.J., Perelet, A., Pardyjak, E., Bowen, G., 2017. Membrane inlet laser spectroscopy to measure H and O stable isotope compositions of soil and sediment pore water with high sample throughput. Rapid Commun. Mass Spectrom. 31, 75–84. https://doi.org/10.1002/rcm.7768.
Phillips, D.L., Gregg, J.W., 2001. Uncertainty in source partitioning using stable isotopes. Oecologia 127, 171–179. https://doi.org/10.1007/s004420000578.
Robertson, J.A., Gazis, C.A., 2006. An oxygen isotope study of seasonal trends in soil water fluxes at two sites along a climate gradient in Washington state (USA). J. Hydrol. (Amst.) 328, 375–387. https://doi.org/10.1016/j.jhydrol.2005.12.031.
Rothfuss, Y., Biron, P., Braud, I., Canale, L., Durand, J.L., Gaudet, J.P., Richard, P., Vauclin, M., Bariac, T., 2010. Partitioning evapotranspiration fluxes into soil evaporation and plant transpiration using water stable isotopes under controlled conditions. Hydrol. Process. 24, 3177–3194. https://doi.org/10.1002/hyp.7743.
Rothfuss, Y., Braud, I., Le Moine, N., Biron, P., Durand, J.L., Vauclin, M., Bariac, T., 2012. Factors controlling the isotopic partitioning between soil evaporation and plant transpiration: assessment using a multi-objective calibration of SiSPAT-Isotope under controlled conditions. J. Hydrol. (Amst.) 442–443, 75–88. https://doi.org/10.1016/j.jhydrol.2012.03.041.
Rothfuss, Y., Merz, S., Vanderborght, J., Hermes, N., Weuthen, A., Pohlmeier, A., Vereecken, H., Brüggemann, N., 2015. Long-term and high frequency non-destructive monitoring of water stable isotope profiles in an evaporating soil column. Hydrol. Earth Syst. Sci. Discuss. 19, 4067–4080. https://doi.org/10.5194/hess-19-4067-2015.
Scanlon, T.M., Kustas, W.P., 2010. Partitioning carbon dioxide and water vapor fluxes using correlation analysis. Agric. For. Meteorol. 150, 89–99. https://doi.org/10.1016/j.agrformet.2009.09.005.
Scanlon, T.M., Sahu, P., 2008. On the correlation structure of water vapor and carbon dioxide in the atmospheric surface layer: a basis for flux partitioning. Water Resour. Res. 44, W10418. https://doi.org/10.1029/2008WR006932.
Schlaepfer, D.R., Ewers, B.E., Shuman, B.N., Williams, D.G., Frank, J.M., Massman, W.J., Lauenroth, W.K., 2014. Terrestrial water fluxes dominated by transpiration: Comment. Ecosphere 5 (5), 61. https://doi.org/10.1890/ES13-00391.1.
Schlesinger, W.H., Jasechko, S., 2014. Transpiration in the global water cycle. Agric. For. Meteorol. 189–190, 115–117. https://doi.org/10.1016/j.agrformet.2014.01.011.
Scott, R.L., Biederman, J.A., 2017. Partitioning evapotranspiration using long-term carbon dioxid e and water vapor fluxes. Geophys. Res. Lett. 44, 6833–6840. https://doi.org/10.1002/2017GL074324.
Scott, R.L., Huxman, T.E., Cable, W.L., Emmerich, W.E., 2006. Partitioning of evapotranspiration and its relation to carbon dioxide exchange in a Chihuahuan Desert shrubland. Hydrol. Process. 20, 3227–3243. https://doi.org/10.1002/hyp.6329.
Sprenger, M., Leistert, H., Gimbel, K., Weiler, M., 2016. Illuminating hydrological processes at the soil-vegetation-atmosphere interface with water stable isotopes. Rev. Geophys. 54, 674–704. https://doi.org/10.1002/2015RG000515.
Sturm, P., Eugster, W., Knohl, A., 2012. Eddy covariance measurements of CO_2 isotopologues with a quantum cascade laser absorption spectrometer. Agric. For. Meteorol. 152, 73–82. https://doi.org/10.1016/j.agrformet.2011.09.007.
Sun, S., Meng, P., Zhang, J., Wan, X., Zheng, N., He, C., 2014. Partitioning oak woodland evapotranspiration in the rocky mountainous area of North China was disturbed by foreign vapor, as estimated based on non-steady-state ^{18}O isotopic composition. Agric. For. Meteorol. 184, 36–47. https://doi.org/10.1016/j.agrformet.2013.08.006.
Sutanto, S.J., Wenninger, J., Coenders-Gerrits, A.M.J., Uhlenbrook, S., 2012. Partitioning of evaporation into transpiration, soil evaporation and interception: a comparison between isotope measurements and a HYDRUS-1D model. Hydrol. Earth Syst. Sci. Discuss. 16, 2605–2616. https://doi.org/10.5194/hess-16-2605-2012.
Sutanto, S.J., van den Hurk, B., Dirmeyer, P.A., Seneviratne, S.I., Röckmann, T., Trenberth, K.E., Blyth, E.M., Wenninger, J., Hoffmann, G., 2014. HESS Opinions "A perspective on isotope versus non-isotope approaches to determine the contribution of transpiration to total evaporation". Hydrol. Earth Syst. Sci. Discuss. 18, 2815–2827. https://doi.org/10.5194/hess-18-2815-2014.
Tarin, T., Yépez, E.A., Garatuza-Payán, J., Watts, C.J., Rodríguez, J.C., Vivoni, E.R., Méndez-Barroso, L.A., 2014. Evapotranspiration partitioning with stable isotopes for ecohydrological studies. Tecnologia y Ciencias del Agua 5, 99–116.
Tsujimura, M., Sasaki, L., Yamanaka, T., Sugimoto, A., Li, S.-G., Matsushima, D., Kotani, A., Saandar, M., 2007. Vertical distribution of stable isotopic composition in atmospheric water vapor and subsurface water in grassland and forest sites, eastern Mongolia. J. Hydrol. (Amst.) 333, 35–46.
van de Griend, A.A., Owe, M., 1994. Bare soil surface resistance to evaporation by vapor diffusion under semiarid conditions. Water Resour. Res. 30, 181–188.
Vargas, A.I., Schaffer, B., Yuhong, L., Sternberg, L.D.L., 2017. Testing plant use of mobile vs immobile soil water sources using stable isotope experiments. New Phytol. 215, 582–594. https://doi.org/10.1111/nph.14616.
Volkmann, T.H., Haberer, K., Gessler, A., Weiler, M., 2016. High-resolution isotope measurements resolve rapid ecohydrological dynamics at the soil-plant interface. New Phytol. 210 (3), 839–849.
Walker, C.D., Brunel, J.P., 1990. Examining evapotranspiration in a semi-arid region using stable isotopes of hydrogen and oxygen. J. Hydrol. (Amst.) 118, 55–75. https://doi.org/10.1016/0022-1694(90)90250-2.
Wang, X.F., Yakir, D., 2000. Using stable isotopes of water in evapotranspiration studies. Hydrol. Process. 14, 1407–1421. https://doi.org/10.1002/1099-1085(20000615)14:8<1407::AID-HYP992>3.0.CO;2-K.
Wang, L., Caylor, K.K., Villegas, J.C., Barron-Gafford, G.A., Breshears, D.D., Huxman, T.E., 2010. Partitioning evapotranspiration across gradients of woody plant cover: assessment of a stable isotope technique. Geophys. Res. Lett. 37, L09401. https://doi.org/10.1029/2010GL043228.
Wang, L., Good, S.P., Caylor, K.K., Cernusak, L.A., 2012. Direct quantification of leaf transpiration isotopic composition. Agric. For. Meteorol. 154–155, 127–135. https://doi.org/10.1016/j.agrformet.2011.10.018.
Wang, L., Niu, S., Good, S., Soderberg, K., McCabe, M.F., Sherry, R.A., Luo, Y., Zhou, X., Xia, J., Caylor, K.K., 2013. The effect of warming on grassland evapotranspiration partitioning using laser-based isotope monitoring techniques. Geochim. Cosmochim. Acta 111, 28–38. https://doi.org/10.1016/j.gca.2012.12.047.
Wang, P., Yamanaka, T., Li, X.-Y., Wei, Z., 2015. Partitioning evapotranspiration in a temperate grassland ecosystem: numerical modeling with isotopic tracers. Agric. For. Meteorol. 208, 16–31. https://doi.org/10.1016/j.agrformet.2015.04.006.
Wang, P., Li, X.-Y., Huang, Y., Liu, S., Xu, Z., Wu, X., Ma, Y.-J., 2016. Numerical modeling the isotopic composition of evapotranspiration in an arid artificial oasis cropland ecosystem with high-frequency water vapor isotope measurement. Agric. For. Meteorol. 230–231, 79–88. https://doi.org/10.1016/j.agrformet.2015.12.063.
Wang-Erlandsson, L., van der Ent, R.J., Gordon, L.J., Savenije, H.H.G., 2014. Contrasting roles of interception and transpiration in the hydrological cycle—part 1: temporal characteristics over land. Earth Syst. Dyn. Discuss. 5 (2), 441–469. https://doi.org/10.5194/esd-5-441-2014.
Wei, Z., Yoshimura, K., Okazaki, A., Kim, W., Liu, Z., Yokoi, M., 2015. Partitioning of evapotranspiration using high-frequency water vapor isotopic measurement over a rice paddy field. Water Resour. Res. 51, 3716–3729. https://doi.org/10.1002/2014WR016737.
Wei, Z., Yoshimura, K., Wang, L., Miralles, D.G., Jasechko, S., Lee, X., 2017. Revisiting the contribution of transpiration to global terrestrial evapotranspiration. Geophys. Res. Lett. 44, 2792–2801. https://doi.org/10.1002/2016GL072235.
Wei, Z., Lee, X., Wen, X., Xiao, W., 2018. Evapotranspiration partitioning for three agro-ecosystems with contrasting moisture conditions: a comparison of an isotope method and a two-source model calculation. Agric. For. Meteorol. 252, 296–310. https://doi.org/10.1016/j.agrformet.2018.01.019.
Welp, L.R., Lee, X., Kim, K., Griffis, T.J., Billmark, K.A., Baker, J.M., 2008. $\delta^{18}O$ of water vapour, evapotranspiration and the sites of leaf water evaporation in a soybean canopy. Plant Cell Environ. 31, 1214–1228. https://doi.org/10.1111/j.1365-3040.2008.01826.x.
Wen, X., Lee, X., Sun, X., Wang, J., Hu, Z., Li, S., Yu, G., 2012. Dew water isotopic ratios and their relationships to ecosystem water pools and fluxes in a cropland and a grassland in China. Oecologia 168, 549–561. https://doi.org/10.1007/s00442-011-2091-0.
Wen, X., Yang, B., Sun, X., Lee, X., 2016. Evapotranspiration partitioning through in-situ oxygen isotope measurements in an oasis cropland. Agric. For. Meteorol. 230–231, 89–96. https://doi.org/10.1016/j.agrformet.2015.12.003.
Wenninger, J., Beza, D.T., Uhlenbrook, S., 2010. Experimental investigations of water fluxes within the soil-vegetation-atmosphere system: stable isotope mass-balance approach to partition evaporation and transpiration. Phy. Chem. Earth 35, 565–570. https://doi.org/10.1016/j.pce.2010.07.016.
Williams, D.G., Cable, W., Hultine, K., Hoedjes, J.C.B., Yepez, E.A., Simonneaux, V., Er-Raki, S., Boulet, G., de Bruin, H.A.R., Chehbouni, A., et al., 2004. Evapotranspiration components determined by stable isotope, sap flow and eddy covariance techniques. Agric. For. Meteorol. 125, 241–258. https://doi.org/10.1016/j.agrformet.2004.04.008.
Wu, Y., Du, T., Ding, R., Tong, L., Li, S., Wang, L., 2017. Multiple methods to partition evapotranspiration in a maize field. J. Hydrometeorol. 18, 139–149. https://doi.org/10.1175/JHM-D-16-0138.1.
Wythers, K.R., Lauenroth, W.K., Paruelo, J.M., 1999. Bare soil evaporation under semi-arid field conditions. Soil Sci. Soc. Am. J. 63, 1341–1349.

Xiao, W., Lee, X., Griffis, T.J., Kim, K., Welp, L.R., Yu, Q., 2010. A modeling investigation of canopy-air oxygen isotopic exchange of water vapor and carbon dioxide in a soybean field. J. Geophys. Res. Biogeosci. 115, G01004. https://doi.org/10.1029/2009JG001163.

Xiao, W., Lee, X., Wen, X., Sun, X., Zhang, S., 2012. Modeling biophysical controls on canopy foliage water 18O enrichment in wheat and corn. Glob. Change Biol. Bioenergy 18, 1769–1780. https://doi.org/10.1111/j.1365-2486.2012.02648.x.

Xiao, W., Lee, X., Hu, Y., Liu, S., Wang, W., Wen, X., Werner, M., Xie, C., 2017. An experimental investigation of kinetic fractionation of open-water evaporation over a large lake. J. Geophys. Res. Atmos. 122, 11651–11663. https://doi.org/10.1002/2017JD026774.

Xu, Z., Yang, H., Liu, F., An, S., Cui, J., Wang, Z., Liu, S., 2008. Partitioning evapotranspiration flux components in a subalpine shrubland based on stable isotopic measurements. Bot. Stud. 49, 351–361. https://doi.org/10.1002/2013JD020260.

Yakir, D., Sternberg, L.D.L., 2000. The use of stable isotopes to study ecosystem gas exchange. Oecologia 123, 297–311. https://doi.org/10.1007/s004420051016.

Yakir, D., Wang, X.F., 1996. Fluxes of CO_2 and water between terrestrial vegetation and the atmosphere estimated from isotope measurements. Nature 380, 515–517. https://doi.org/10.1038/380515a0.

Yamanaka, T., Tsunakawa, A., 2007. Isotopic signature of evapotranspiration flux and its use for partitioning evaporation/transpiration components. Tsukuba Geoenviron. Sci. 3, 11–21.

Yamanaka, T., Yonetani, T., 1999. Dynamics of the evaporation zone in dry sandy soil. J. Hydrol. (Amst) 217, 135–148.

Yang, B., Wen, X., Sun, X., 2015. Seasonal variations in depth of water uptake for a subtropical coniferous plantation subjected to drought in an East Asian monsoon region. Agric. For. Meteorol. 201, 218–228. https://doi.org/10.1016/j.agrformet.2014.11.020.

Yepez, E.A., Williams, D.G., Scott, R.L., Lin, G.H., 2003. Partitioning overstory and understory evapotranspiration in a semiarid savanna woodland from the isotopic composition of water vapor. Agric. For. Meteorol. 119, 53–68. https://doi.org/10.1016/S0168-1923(03)00116-3.

Yepez, E.A., Huxman, T.E., Ignace, D.D., English, N.B., Weltzin, J.F., Castellanos, A.E., Williams, D.G., 2005. Dynamics of transpiration and evaporation following a moisture pulse in semiarid grassland: a chamber-based isotope method for partitioning flux components. Agric. For. Meteorol. 132, 359–376. https://doi.org/10.1016/j.agrformet.2005.09.006.

Yepez, E.A., Scott, R.L., Cable, W.L., Williams, D.G., 2007. Intraseasonal variation in water and carbon dioxide flux components in a semiarid riparian woodland. Ecosystems 10, 1100–1115.

Yuan, G.F., Zhang, N., Sun, X.M., Wen, X.F., Zhang, S.C., 2010. Partitioning wheat field evapotranspiration using Keeling Plot method and continuous atmospheric vapor $\delta^{18}O$ data (in Chinese). Chinese J. Plant Ecol. 34, 170–178.

Zhang, S., Wen, X., Wang, J., Yu, G., Sun, X., 2010. The use of stable isotopes to partition evapotranspiration fluxes into evaporation and transpiration. Acta Ecol. Sin. 30, 201–209. https://doi.org/10.1016/j.chnaes.2010.06.003.

Zhang, Y., Shen, Y., Sun, H., Gates, J.B., 2011. Evapotranspiration and its partitioning in an irrigated winter wheat filed: a combined isotopic and micrometeorologic approach. J. Hydrol. (Amst.) 408, 203–211. https://doi.org/10.1016/j.jhydrol.2011.07.036.

Zhang, Y., Peña-Arancibia, J.L., McVicar, T.R., Chiew, F.H.S., Vaze, J., Liu, C., Lu, X., Zheng, H., Wang, Y., Liu, Y.Y., Miralles, D.G., Pan, M., 2016. Multi-decadal trends in global terrestrial evapotranspiration and its components. Sci. Rep. 6, 19124. https://doi.org/10.1038/srep19124.

Zhou, S., Yu, B., Zhang, Y., Huang, Y., Wang, G., 2016. Partitioning evapotranspiration based on the concept of underlying water use efficiency. Water Resour. Res. 52, 1160–1175. https://doi.org/10.1002/2015WR017766.

Zimmermann, U., Münnich, K.O., Roether, W., Kreutz, W., Schubach, K., Siegel, O., 1966. Tracers determine movement of soil moisture and evapotranspiration. Science 152, 346–347.

Zimmermann, U., Ehhalt, D., Münnich, K.O., 1967. Soil-water movement and evapotranspiration: changes in the isotopic composition of the water. Proceedings of the Symposium of Isotopes in Hydrology 567–584.